UNIVERSIDAD DE CHILE
FACULTAD DE CIENCIAS FÍSICAS Y MATEMÁTICAS
DEPARTAMENTO DE GEOLOGÍA

SPATIAL DISPOSITION SIMULATION OF ALTERATION ZONES BASED ON CELLULAR AUTOMATA

MEMORIA PARA OPTAR AL TÍTULO DE
GEÓLOGO

JORGE ENRIQUE VEGA GARCÍA

PROFESOR GUÍA:
FELIPE NAVARRO VARGAS

MIEMBROS DE LA COMISIÓN:
DANIEL MONCADA DE LA ROSA
KATJA DECKART

Este trabajo ha sido parcialmente financiado por Advanced Laboratory for Geostatistical Supercomputing

SANTIAGO DE CHILE
2019

RESUMEN DE LA MEMORIA PARA OPTAR
AL TÍTULO DE GEÓLOGO
POR: JORGE ENRIQUE VEGA GARCÍA
FECHA: 2019
PROF. GUÍA: FELIPE NAVARRO VARGAS

SPATIAL DISPOSITION SIMULATION OF ALTERATION ZONES BASED ON CELLULAR AUTOMATA

Debido a la creciente dificultad y costos asociados a la exploración y operación en la minería, modelos numéricos basados en diferentes metodologías son cada vez más comunes en la simulación de procesos geológicos complejos. Es por esto que a principios del año 2018 ALGES inicia el proyecto Simulación de Disposición Espacial y de Zonación de Alteraciones de un Pórfido Cuprífero Basada en Autómatas Celulares. Este proyecto busca simular a través de sistemas numéricos el emplazamiento espacial y zonación de alteraciones hidrotermales en un sistema de pórfido cuprífero con una litología y contexto estructural definidos para así poder desarrollar una herramienta de guía en la exploración minera. Esta modelación numérica se basa en autómatas celulares, metodología ya usada en modelamiento minero.

El objetivo principal de este trabajo es simular a través de un modelo computacional discreto, la distribución espacial y las zonaciones de alteraciones hidrotermales de un sistema de pórfido cuprífero. Este objetivo se desarrolla a través del modelamiento de la variación de pH de un fluido que fluye por una grilla porosa de roca. Debido a esta interacción de fluido/roca, también se simula la variación de porosidad en la roca a lo largo del tiempo. Además, se analiza la variación termal de un fluido cuando este fluye a través de una roca caja con una temperatura distinta. La validación de este modelo se adquiere al comparar los resultados de las simulaciones con los modelos tradicionales de pórfido cuprífero. A través de los resultados adquiridos se espera producir datos cualitativos con los cuales comparar los modelos tradicionales.

El trabajo comienza introduciendo el marco teórico en el cual se explica en qué consiste un modelo geológico. Luego se dan a conocer los modelos tradicionales de pórfido cuprífero junto con los tipos de alteraciones hidrotermales asociados a estos. Se realiza una introducción a los modelos computacionales en general, con hincapié en el tipo de modelo usado en este trabajo (autómatas celulares). Se contextualizan las aplicaciones de estos modelos computacionales en la geología y se mencionan algunos ejemplos.

El modelo es generado usando el lenguaje de programación Python, utiliza una programación orientada a objetos y está basado en autómatas celulares. El modelo propuesto consiste en grillas que interactúan entre sí de acuerdo a tres relaciones principales. Estas relaciones son el intercambio térmico, variación de pH y la posición del fluido. Basado en estas variables un mapa de zonas de alteración es generado.

Los resultados de las simulaciones realizadas sobre el modelo generado difieren levemente a lo que se encuentra en modelos de pórfido cuprífero tradicionales. Esto se asocia a la simplificación de la variabilidad de algunas constantes termales el dominio por sobre el cual ciertas relaciones están definidas.

RESUMEN DE LA MEMORIA PARA OPTAR
AL TÍTULO DE GEÓLOGO
POR: JORGE ENRIQUE VEGA GARCÍA
FECHA: 2019
PROF. GUÍA: FELIPE NAVARRO VARGAS

SPATIAL DISPOSITION SIMULATION OF ALTERATION ZONES BASED ON CELLULAR AUTOMATA

Due to the growing difficulty and expenses associated to mineral exploration and mine operation, numerical models based on different methodologies are progressively more common when modeling complex geological processes. Responding to these needs, on 2018 ALGES starts the project named Spatial Disposition Simulation of Alteration Zones Based on Cellular Automata. This project seeks to simulate how a hydrothermal generates the alteration zones of a porphyry copper system through a numerical system. This numerical modeling is based on cellular automata which has been previously used in mining modeling.

The main objective of this project is to simulate through a discrete computer model the spatial distribution and the zoning of hydrothermal alterations in a porphyry copper system. This is achieved through the modeling of the pH variation of a fluid that flows through a porous rock grid. The porosity variation of the rock grid is also modeled together with the thermal variations associated to the heat exchange between the fluid and the rock. This model is validated by comparing it to traditional porphyry copper models.

This thesis starts by introducing the theoretical framework in which the concept of geological model is explained. Traditional porphyry copper models are introduced as well to provide contextualization. The concepts of computer models and simulations are introduced, focusing on discrete models specifically cellular automata.

The model is created in Python programming language, uses object-oriented programming and is based on cellular automata. The proposed model consists in grids that interact with each other according to three main relationships. These relationships are thermal exchange, pH variation and the fluid's position. Based on these variables an alteration zone map is generated.

The results of the simulations done over the generated model slightly differ to what is found in traditional porphyry copper models. This is associated to the simplification of the variability of some thermal constants and the domain in which some relationships are defined.

Agradecimientos

Agradezco a mis padres por inculcarme el deseo de aprender. A mi tata Sergio por apoyarme todos estos años y siempre estar ahí. A mi hermano Camilo por ser mi motor y gran amigo de la vida.

A Pamela por acompañarme por esta montaña rusa de stress y emociones que significa trabajar en la memoria, gracias por tu incondicional apoyo. A mis amigos de la terraza, del departamento, de North Bergen y de la vida por siempre escucharme.

Agradezco a los profesionales de ALGES en especial a mi profesor guía Felipe Navarro por darme esta oportunidad. También agradezco a Gonzalo Díaz, que sin tus palabras de aliento y contribuciones al proyecto esto no hubiese sido posible.

Finalmente, agradezco a la vida por haberme dado las oportunidades que se me han dado. No todos con los que crecí han podido convertirse en profesionales aunque hayan tenido las capacidades intelectuales para hacerlo. Espero representar bien mis vivencias, lugares y especialmente personas con las que he convivido.

Contents

List of Tables

List of Figures

Chapter 1

Introduction

Exploration in the mining industry has become progressively more competitive with time. The most evident deposits have been already studied and exploited. It is expected that the future discoveries of mineral deposits will require more sophisticated technology than the one implemented in traditional mineral prospecting (Hronsky, 2015). The growing difficulty of finding new economically relevant districts, in addition to the high costs associated with diamond drilling, has influenced the mining industry to find new ways of optimizing processes. Consequently, computational modeling is being heavily used in the different stages of mineral exploration and production.

Focusing on the national context, the mining industry has a central role in the country's productivity and accounts for at least 6% of Chile's GDP (SERNAGEOMIN, 2018). Of all the mineral exports, copper can be considered the "Jewel in The Crown" for the Chilean economy. According to national reports, in 2017 alone Chile produced more than 5,500 metric tons of copper which accounts for around 27% of the global production of the "red metal" (*Producción cobre de mina mundial y Chile*, 2018).

One of the most studied kind of copper deposits is the porphyry copper type. Porphyry copper systems supply about three quarters of the worlds copper, half the molybdenum, about one fifth of the gold, most of the rhenium, and minor amounts of other metals including silver, palladium, tellurium, selenium, bismuth, zinc and lead (Sillitoe, 2010). Starting in the middle of the twentieth century, porphyry copper systems have been schematically modeled. These models include their spatial disposition and their hydrothermal alteration zones. This was made possible through field observations and the study of different thermodynamic and mineralogical characteristics. These porphyry copper models have made mineral exploration more efficient and also supply a guide of where and how to continue exploring or mining. The present models of this type of deposit are based on hydrothermal alteration zoning which have a spatial relationship among them. The spatial relationship of these zones help defining exploration vector when a specialist distinguishes them in the field.

Traditional porphyry copper models are defined as large volumes ($10 \rightarrow 100$ km^3) of hydrothermally altered rock centered around a stock (magmatic intrusion) (Sillitoe, 2010). To better understand this definition it is necessary to first understand the terms used. Hydrothermal systems consist in sets of processes that redistribute energy and mass in response to the circulation of aqueous fluids (hydrothermal fluids) (Norton, 1984). Hydrothermal fluids are aqueous solutions with generally multiple dissolved gases (most importantly CO_2, H_2S, CH_4), and NaCl (Drummond, 1981). These fluids are heated naturally through diverse crustal and mantle geological processes including like basinal fluid interaction, magmatic differentiation and mantle degassing (Kumar & Srivastava, 2014). Hydrothermal fluids generate mineralogical variations in the host rock they penetrate. These variations are known as hydrothermal alterations. Hydrothermal alterations consist in chemical replacement of the original minerals in a rock by new minerals where a hydrothermal fluid delivers the chemical reactants and removes the aqueous reaction products (Reed, 1997). In other words, a porphyry copper deposit consists in a host rock altered physically and chemically by an aqueous fluid that originated from a magmatic intrusion.

Traditional geological models, although of great relevance for mineral exploration, have certain limitations due to the fact that they represent deposits schematically. The main predicament that these schematic models present is the fact that they are idealized systems based on data compilation from multiple porphyry deposits around the world. These models cannot be applied across different deposits with high precision because the structural and lithological characteristic of each deposit vary. Due to these different characteristics, deposits can have different geometries and disposition of hydrothermal alteration zoning.

Due to the large variety of porphyry copper deposits found around the world, it is compelling to study the spatial disposition and hydrothermal alteration zones development of a system with a fixed lithology and rock structures. This makes analyzing economically interesting zones possible based on parameters like temperature of mineral formation, depth and pH. These parameters control the different mineral assemblages found in hydrothermal alterations associated to hydrothermal systems. The porphyry copper system zoning has been well documented, studied and characterized in literature (Sillitoe, 2000, 1973; Lowell, 1968; Hemley, Meyer, Hodgson, & Thatcher, 1967; Walker, 1963; Corbett & Leach, 1998), which provides a great quantity of valuable information that enables modeling of hydrothermal systems.

Consequently in the year 2018, under the program of developing computational models to simulate geologic phenomena, the Advanced Laboratory for Geostatistical Supercomputing (ALGES) part of the Advanced Mining Technology Center (AMTC) of the Universidad de Chile proposes the project of developing a porphyry copper system simulator to analyze how these systems evolve and stabilize.

1.1 Research Formulation

As previously mentioned, porphyry copper deposits are responsible for most of the global copper production. These deposits are quite common in Chile, as seen in figure 1.1, and are relevant to the metal production. Some of the most important examples of these kinds of deposits are Escondida, Collahuasi, Chuquicamata, Escondida, Los Bronces and El Teniente. Thus, given the economic importance of these systems and the complexity of their anatomy, it is compelling to study them from a computational simulation lens.

A computational simulation of this type of deposit would allow to study the distribution of interest zones within a porphyry copper system. Given the vast study already done on this topic from a traditional geologic view, all the knowledge of how these systems are born and evolve could be implemented in a numerical model of the multiple phenomena found in the formation of these deposits. Motivated by this initiative, the experts at ALGES proposed the development of such numerical simulation so that it can be used in future of the mining industry in Chile and the world.

Due to the previous experience the ALGES team had with cellular automata (CA) (Miranda, 2017), this methodology was proposed. This is an innovative manner of modeling the study due to the effectiveness these dynamic systems deal with local interactions. These systems are defined over a grid within which each cell possesses a starting state which is modified by the interaction with its neighbors (Roy, 2019). In this case the grid will represent a host rock which is modified when in contact with a hydrothermal fluid. In this case the cellular automata will consist of two grids (a rock grid and a hydrothermal fluid grid) interacting with each other modifying each other's cells. In the following chapters the phenoma taken into account are explained as well as their variation and the numerical formulas associated with them.

1.2 Main Objective

Simulate through a discrete computer model the spatial distribution and hydrothermal alteration zones of a porphyry copper system with a defined lithology and structural setting.

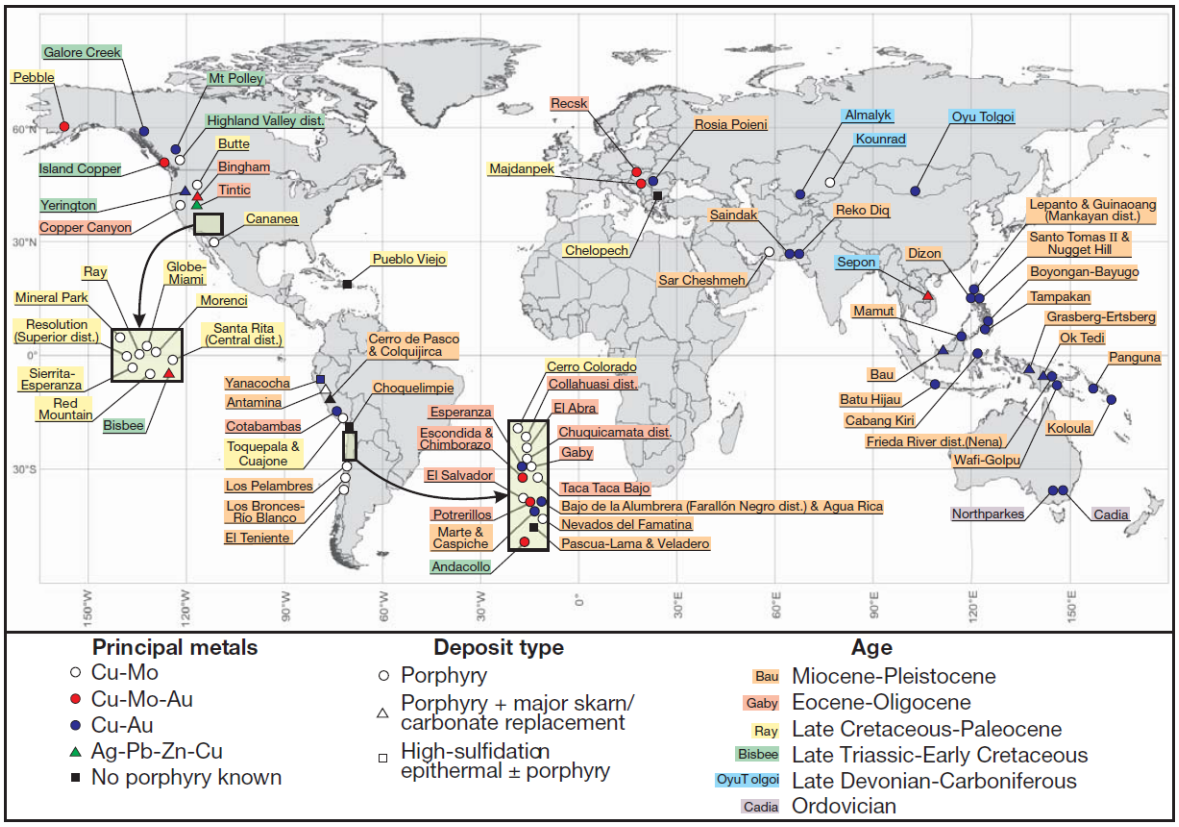

Figure (1.1) Known porphyry copper deposits in the world, adopted from (Sillitoe, 2010).

1.3 Specific Objectives

The specific objectives necessary to achieve the main objective of this project are:

- Model the pH variation of a hydrothermal fluid that flows through a rock grid.
- Simulate the porosity variation due to the interaction of the hydrothermal fluid with a defined host rock.
- Analize the thermal variation of a hydrothermal fluid when it flows through a host rock with a different temperature.
- Produce data to validate models found in literature.
- Propose qualitative validations of the simulated parameters.

1.4 Reader's Guide

In order to ease the comprehension of this document, the topics of each chapter are summarized in the following paragraphs.

Chapter 1: Introduction to the general study of this document in which objectives are stated and a general guide is provided.

Chapter 2: The theoretical background of the document is explained in further detail. Here the models on which the proposed simulation is based on are explained. The chapter begins introducing the geological models used to construct the simulation and ends with an introduction to computer generated models as well as how simulations have been used in geology.

Chapter 3: Full description of the numerical model developed to achieve the main objective. Describes the simulation algorithm and how it is organized.

Chapter 4: Describes the initialization of the model as well as the code associated with the entire simulation process. This chapter also describes in full detail how each cell state evolves.

Chapter 5: Describes the different experiments performed to the numerical simulation as well as their results.

Chapter 6: Discusses the experiments' results as well as how the model compares and contrasts to the traditional porphyry copper systems models and real life deposits.

Chapter 7: States what can be concluded from this document and proposes new studies to further the improvement of the algorithm.

Chapter 2

Theoretical Framework

The present work proposes algorithms that reproduce a geological model for a mineral deposit through cellular automata. Now the theoretical framework of these geological models, in addition to the computational methodologies used for the completion of this work, will be explained. Examples of other instances where algorithms are used to model phenomena pertaining to geology will also be explained for contextualization in the field.

2.1 Geological Models

Geological models are spatial representations of the distribution of sediments, rocks, fluids, and/or other components below earth's surface. These models attempt to explain different phenomena that occur in our planet ranging from metamorphic grades (Spear & Spear, 1993) to basin depositional history and deformation (Amilibia et al., 2008). The models analyzed in this work relate specifically to porphyry copper deposits, their genesis, spatial distribution and thermodynamic controls.

2.1.1 Porphyry Copper Models

Starting on the first half of the twentieth century porphyry copper deposits has been closely studied by geoscientists. In the 1920s it was noted that these types of deposits are closely related to magmatic activity typically of intermediate to felsic composition (Emmons, 1927). These models advanced through the studies of vein formation and wall-rock alteration (Meyer, 1957, 1965), which allowed the development of the geological models used as a framework to create the work presented in this document. The present understanding of the genesis of porphyry copper deposits is based mainly on geologic observations combined with geochemical, mineralogical, structural, petrological, geophysical and geochronological data. This work will mainly focus on results obtained from geochemical experiments (Reed, 1997; Smith, Naden, Jenkin, & Keith, 2017) and the thermodynamic parameters of different hydrothermal alterations.

Geological Setting of a Porphyry Copper Deposit

Porphyry copper deposits are encountered mainly near magmatic arcs subjected to regional stress regimes that range from moderately extensional, oblique slip to contractional (Tosdal & Richards, 2001). Empirical data suggests that there is a more direct correlation between these kind of deposits and contractional settings characterized by crustal thickening, surface uplift and rapid exhumation (Sillitoe, 2010) as seen in places like the Central Andes, Iran, the Philippines and southwestern North America, see figures 1.1 and 2.1. These deposits are spatially and genetically related to passively emplaced hypabysal intermediate to felsic stocks which become saturated in water as they intrude and while their outer parts undergo crystallization they release fluids which produce alteration and mineralization (Sillitoe, 1972).

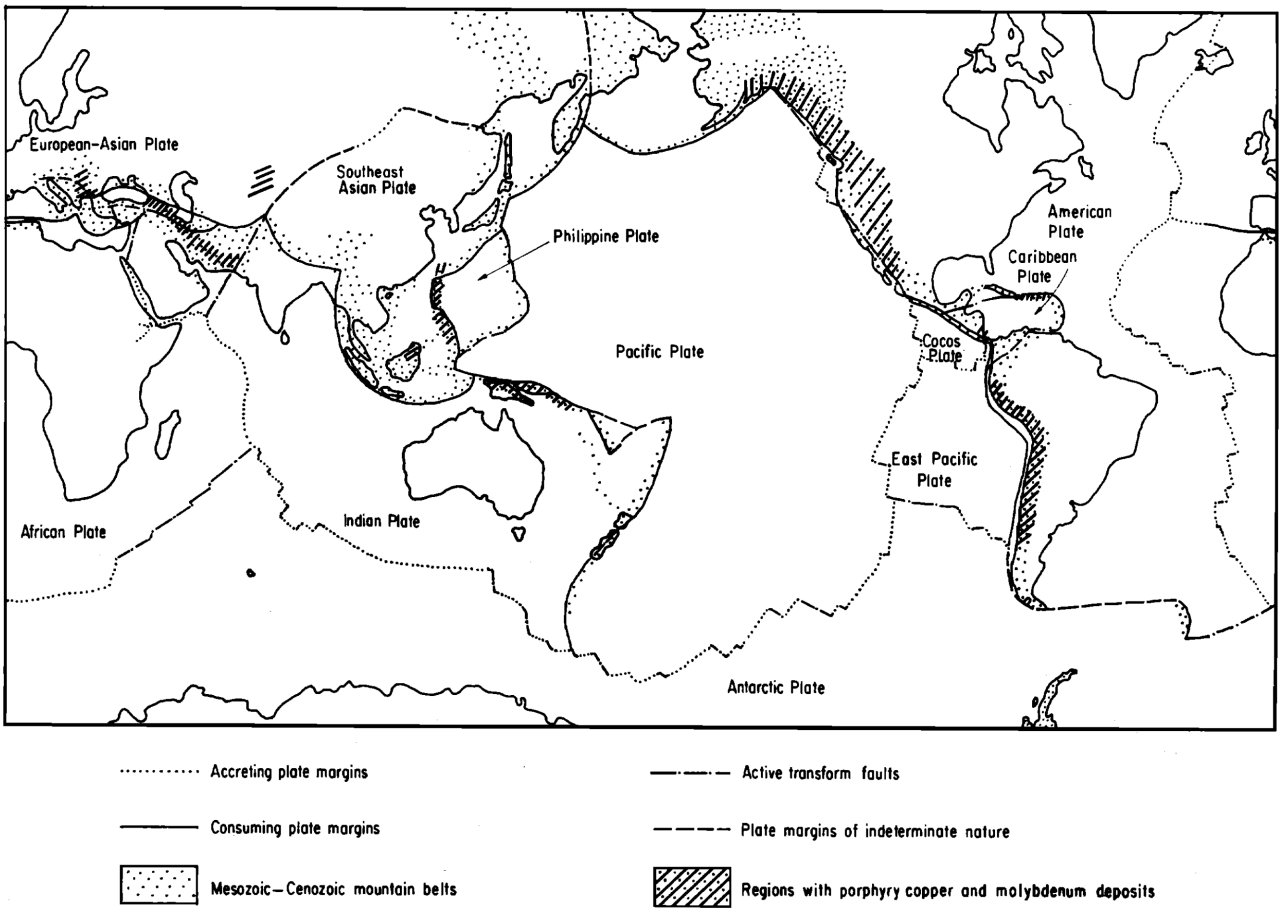

Figure (2.1) Distribution of porphyry copper deposits according to tectonic settings, adopted from (Sillitoe, 1972).

Porphyry copper systems tend to be found in linear belts parallel to large orogens like the Andes (R. H. Sillitoe & Perelló, 2005), as seen in figure 2.2. This characteristic has been described as early as the nineteenth century (Domeyko, 1876) and has been a feature that helped mineral exploration in the Central Andes especially during the 1980s and 1990s (R. H. Sillitoe & Perelló, 2005). Each belt is associated with a magmatic arc dimensionally similar to the belt with an usual extension of 5 to 30 km across or in length (Sillitoe, 2010). Tectonically, given the fact that porphyry copper deposits are associated with orogenic belts characterized by calc-alkaline magmatism (Sillitoe, 1972), these deposits are mainly confined to subduction zones where oceanic plates underthrust adjacent continental plates.

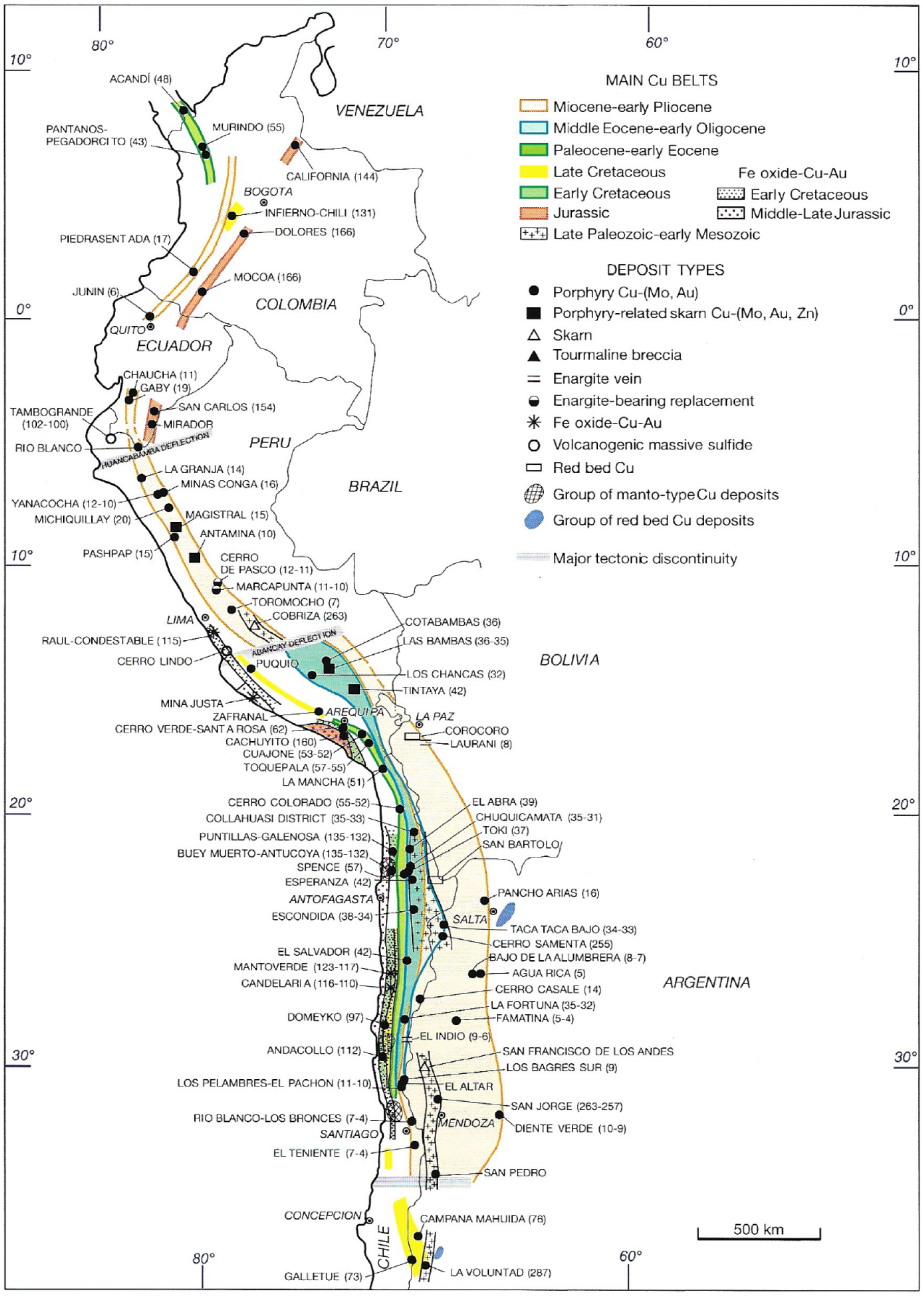

Figure (2.2) Copper belts along the Andes and relevant deposits, adopted from (R. H. Sillitoe & Perelló, 2005).

Architecture of a Porphyry Copper Deposit

As mentioned in the previous chapter, porphyry copper models consist of hydrothermally altered rock centered around a stock of felsic to intermediate composition. This means that one can define zones of different types of hydrothermal alterations with respect to the magmatic intrusion. One of the earliest conceptual models of the different alteration zones is the one postulated by Lowell and Guilbert (1970) seen in figure 2.3 which was postulated based on the field observations of the Kalamazoo orebody in Arizona (Lowell, 1968). As seen in figure 2.3, the zones consist of different types of hydrothermal alteration assemblages. Hydrothermal alterations are the result of a specific fluid temperature and pH range as well as a determined depth and water/rock ratio. The water/rock ratio corresponds to how much hydrothermal fluid is in contact with the host rock, specifically the mass of fluid phase in contact with rock per the mass of rock in that volume (Alt-Epping & Smith, 2001). More recent studies have characterized these types of deposits to a greater extent. As seen in figure 2.4 Sillitoe ((2010)) is the most widely accepted conceptual model of porphyry copper deposits. The general understanding of these models suggest that the average lifespan of a hydrothermal system associated with an Andean porphyry copper deposit is between 2.5 to 4 million years (Sillitoe & Mortensen, 2010). For a better understanding and characterization of these zones the different alterations will be described next.

Potassic Alteration Potassic alteration is characterized by a mineralogy consisting of potassium feldspar and/or biotite. Accessory minerals also include quartz, sericite, chlorite (Reed, 1997). This corresponds to a high temperature alteration ranging from 400 to 600 °C. The pH conditions under which this assemblage is obtained range from neutral to alkaline and the depth associated with this alteration corresponds to a porphyry depth (Corbett & Leach, 1998). Porphyry depth corresponds to anything greater than 3660 [m] below surface (Lindgren, 1933). Potassic alteration are economically relevant because it is upon the potassic–sericitic interphase where the copper sulfides (primary copper ore in porphyries) occur (Lowell & Guilbert, 1970).

Propylitic Alteration This alteration has a mineral assemblage consisting of albite, chlorite and epidote is the result of small water/rock ratios, low temperatures (200-350 °C) and near neutral pH conditions (neutral to alkaline) (Reed, 1997). Propylitic assemblages occur at mesothermal depths (Corbett & Leach, 1998) which corresponds to depths ranging from 1219-3660 [m] (Lindgren, 1933). These alterations might also include actinolite, diopside and andraditic garnet which indicates higher temperatures (280-300 °C).

Sericitic Alteration Sericitic alterations are characterized by quartz, sericite, pyrite and chlorite assortments. They occur in large halos around porphyry copper deposits (Reed, 1997). Sericitic alteration is one of the most abundant alteration assemblages as it is present in nearly all types of hypogene ore deposits in aluminous rocks, as well as in gold-quartz and massive sulfide systems, but most importantly (for the case-study) it is present in some supergene environments such as porphyry copper deposits (Meyer, 1967). This alteration occurs under pH conditions ranging from 5 to 6, temperatures higher than 100 °C and

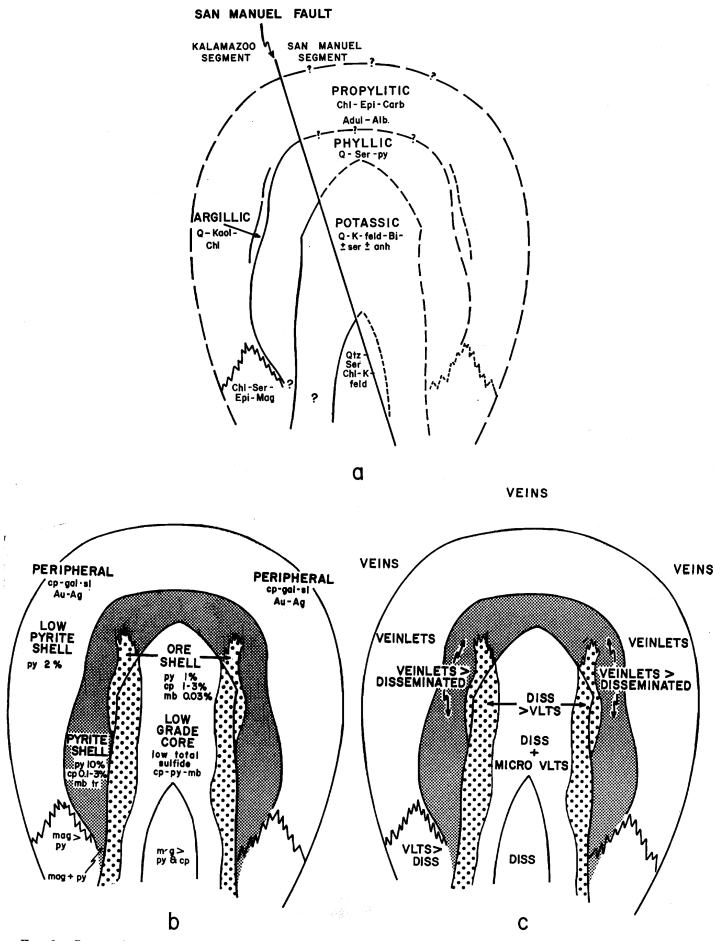

Figure (2.3) Concentric alteration-mineralization zones at San Manuel–Kalamazoo., adopted from (Lowell & Guilbert, 1970). This model corresponds to one of the most traditional characterizations of a porphyry copper system.

mesothermal and porphyry depths (Corbett & Leach, 1998) which corresponds to depths greater than 1220 [m] (Lindgren, 1933). Sericitic alteration assemblages consist mainly in clay minerals. Each clay mineral or pairing of these minerals specifies temperature ranges. Illite–smectite corresponds to 100-200 °C; illite by itself indicates 200-250 °C; sericite alone represents a temperature range from 250-450 °C; and although not clay minerals, corundum and andalusite indicate a temperature greater than 450 °C (Corbett & Leach, 1998).

Intermediate Argillic Characterized by smectite and kaolinite (usually replacing plagioclase) and other montmorillonite-group minerals, this alteration zone commonly grades zonally to propylitic alteration towards fresh rock and to sericitic alteration towards a vein (Meyer, 1967). The mineral assemblage of this alteration zone might also contain alunite as an accessory and may also be zoned internally with montmorillonite clays more common near the distal areas and kaolin minerals towards the inner areas (Meyer, 1967). This alteration occurs at pH of 4-5 and 3-4 if it contains alunite; the temperature corresponds to a range of 150-300 °C (Corbett & Leach, 1998) and are formed at epithermal depths (less than 1200 [m]) (Lindgren, 1933). The intermediate argillic alteration zone usually develops veinward from the propylitic alteration zone and outside the sericitic zone, but it can also be found

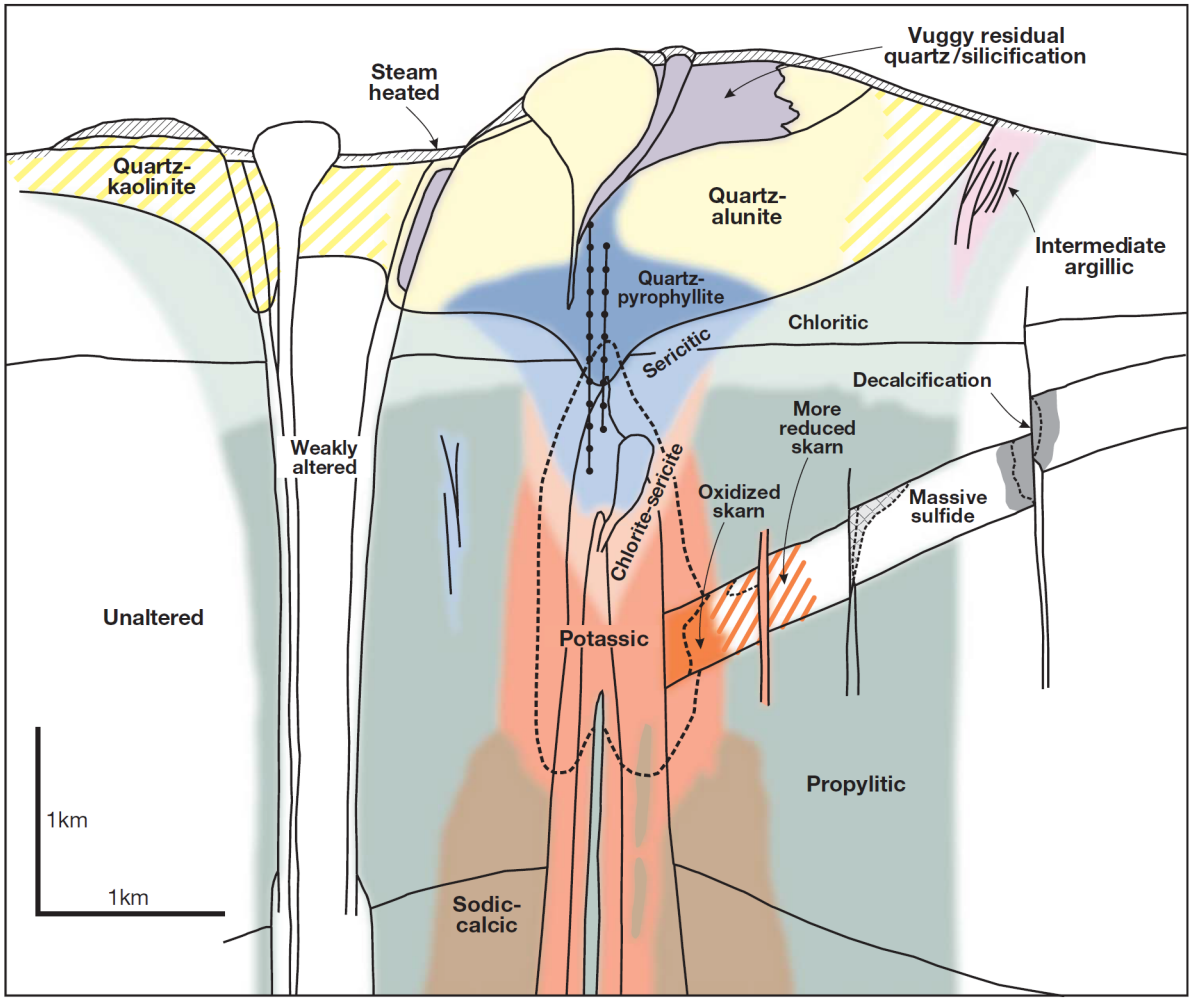

Figure (2.4) Generalized alteration-mineralization zoning pattern for porphyry Cu deposits adopted from (Sillitoe, 2010). This model corresponds to one of the most updated widely accepted model.

not in between them (Reed, 1997).

Advanced Argillic Quartz and dickite are the main minerals in the advanced argillic mineral assemblage which also may contain kaolinite, pyrophyllite, pyrite, alunite, zunyite, topaz and is associated with covellite–enargite–gold epithermal deposits (Reed, 1997). This type of alteration is found as an inner or veinward zone adjoining multiple base-metal veins, telescoped pipes, or porphyry copper deposits associated with granodiorites in volcanic fields (Meyer, 1967). These zones are usually found, although not restricted to, upper parts of porphyry copper systems. These shallow levels of pervasive advanced argillic alterations are known as lithocaps which can be associated to an underlying porphyry copper deposit (Sillitoe, 2010). Advanced argillic zones can develop at varied depths as well as a wide range of temperatures, encompassing the ranges stated for other alteration zones. What characterizes this zone is the low pH under which it develops. This alteration has a pH range of 1-3.5, although alunite indicates a pH greater than 2 and an exclusive quartz predominance is associated with a pH lower than 1 (Corbett & Leach, 1998).

A schematic diagram of the different hydrothermal alterations previously described can be seen in figure 2.5. This figure also shows the mineralogy at different pH, temperature and depth ranges.

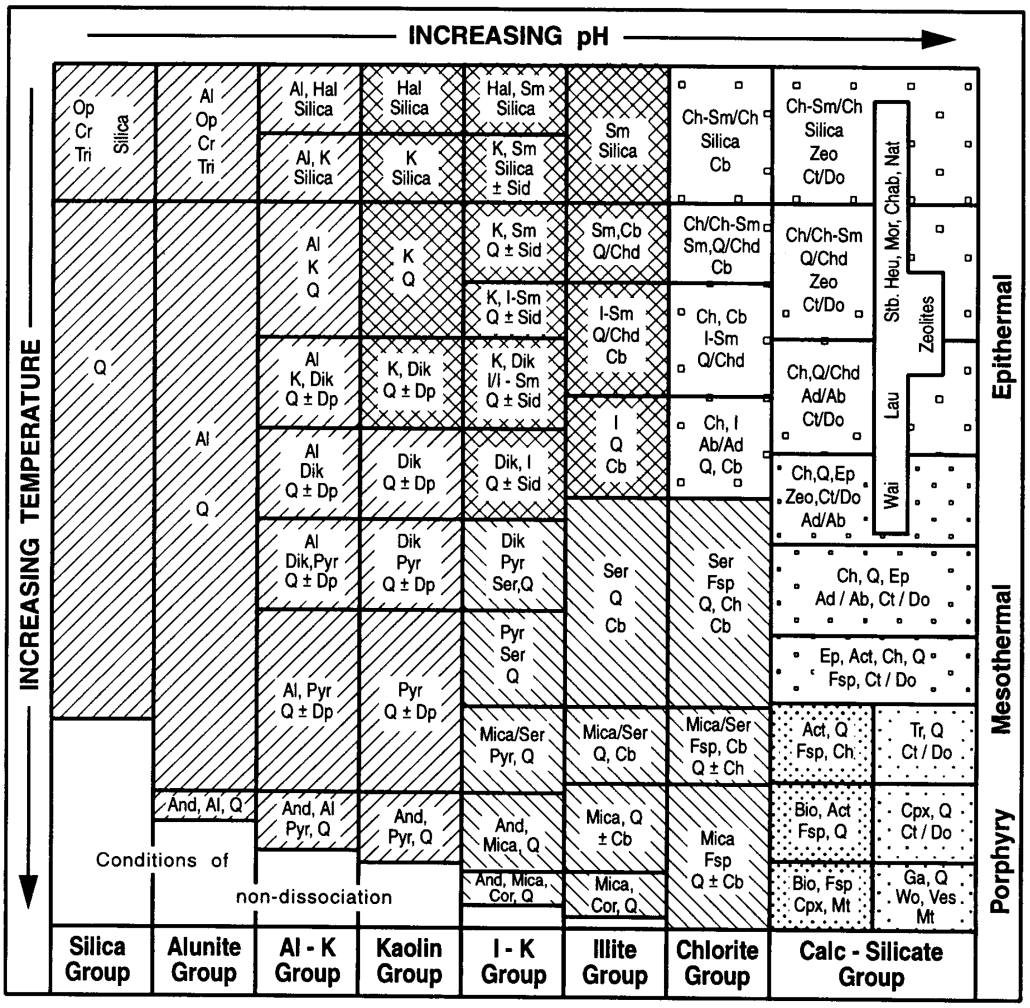

Mineral Abbreviations :

Ab - albite; Act - actinolite; Ad - adularia; Al - alunite; And - andalusite; Bio - biotite; Cb - carbonate (Ca, Mg, Mn, Fe)
Ch - chlorite; Chab - chabazite; Chd - chalcedony; Ch-Sm - chlorite-smectite; Cor - corundum;
Cpx - clinopyroxene; Cr - cristobalite; Ct - calcite; Do - dolomite; Dik - dickite; Dp - diaspore; Ep - epidote;
Fsp - feldspar; Ga - garnet; Hal - halloysite; Heu - heulandite; I - illite; I-Sm - illite-smectite; K - kaolinite;
Lau - laumontite; Mt - magnetite; Mor - mordenite; Nat - natrolite; Op - opaline silica; Pyr - pyrophyllite;
Q - quartz; Ser - sericite; Sid - siderite; Sm - smectite; Stb - stilbite; Tr - tremolite; Tri - tridymite;
Ves - vesuvianite; Wai - wairakite; Wo - wollastonite; Zeo - zeolite

Potassic
Propylitic
Outer / Sub Propylitic
Skarn
Argillic
Advanced Argillic
Phyllic

Figure (2.5) Common hydrothermal alteration mineralogy associated with pH, temperature and depth ranges in hydrothermal systems. Adopted from (Corbett & Leach, 1998).

Temporality of the Hydrothermal Fluid's Conditions

The formation of these hydrothermal alterations has a direct relationship with the state of the fluid that generates them. The fluid responds to the stage of the magmatic intrusion that it is generated from. Therefore, as the magma progressively solidifies and cools through time, the hydrothermal fluid's conditions change. At early stages magma is present at the top of the parental magma chamber which generates a single-phase, low to moderate salinity liquid that undergoes phase separation to generate immiscible hypersaline liquid and vapor. This fluid is associated with the potassic alteration. The low pressure vapor that escapes forms acidic condensate to produce advanced argillic alteration (Sillitoe, 2010). As magma solidification advances, the system progressively cools to temperatures of around 400°C. Under these conditions sericitic alterations begin to form from a single phase aqueous liquid. This process can be observed in figure 2.6.

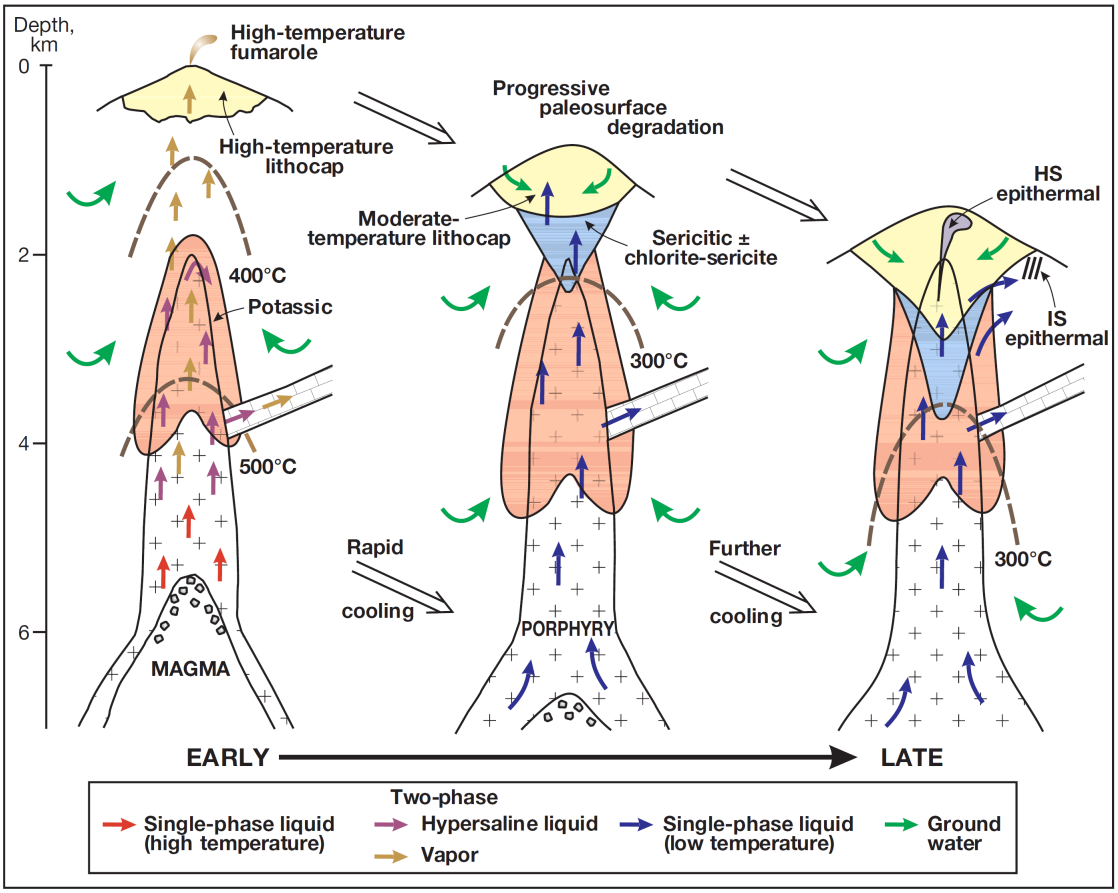

Figure (2.6) Evolution of the main magmatic fluid and alteration types according to the cooling of the associated magma chamber. Adopted from (Sillitoe, 2010).

2.2 Computer Based Models

Models are usually simplifications of real-life phenomena which arise from the analysis of the different variables that affect a system and the relationships between these variables (Rocca,

2005). A system can be considered as a set of elements whose interactions is of interest. In other words, models are sets of rules that attempt to recreate the conditions and relationships of a real life case-study. With an established model one can simulate an outcome based on initial conditions. Therefore, a simulation attempts to obtain predictions of how a system will evolve or stabilize given specific conditions or a hypothesis. The simulation will produce the best fitting outcome to a proposed scenario.

There are different types of models which can broadly be grouped in the following categories (Rocca, 2005):

- Dynamic models: These are used to represent systems in which the state does not change with time.
- Static models: Utilized to represent systems which do not change with time.
- Continuous models: Represent systems that changes gradually and the variables that affect the system are continuous.
- Discrete models: These models are based on step by step interactions. Variables are treated discontinuously.
- Deterministic models: Models in which the outcome for specific conditions is unique and always the same.
- Stochastic models: Utilized to represent systems in which the outcome is not always the same. The interactions between variables does not always yield the same product.

It is possible to implement mixed models, for example, treat some variables within the model analytically and others numerically. These models can be concocted physically (through scaled models), analytically (through mathematical equations) or numerically (in which a defined equation is not obtained, only the numerical behavior of the variables). Computer based models can be designed with any of these methodologies except the physical model (scaled model).

Based on a model one can start simulating a system in order to predict outcomes or even to generate understanding of outcomes already obtained. There are different ways in which a simulation can be carried out. Most commonly simulations can be equation-based or agent-based. Equation-based simulations can be applied where there is a governing theory guides the construction of mathematical models, while agent based simulations focuses on individual interactions of individual agents (Winsberg, 2019). Another common type of simulating phenomena is through Monte Carlo simulations which consist on computer algorithms that utilize randomness to calculate the properties of a model, although the randomness of the algorithm is not a feature of the target model (Winsberg, 2019).

2.2.1 Cellular Automata

Discrete models may also be applied to continuous phenomena (Hall, 1986) and there are multiple kinds of this type of model. Cellular automata are mathematical idealizations of physical systems in which time, space and physical quantities' values are discrete. These systems consist of regular form lattices (arrays) with a discrete variable at each site which are known as cells. Each cell has a specified initial state of variables, which evolves in discrete time steps based on interactions with their neighbors' (other cells) status and a defined set of rules that govern these interactions (Wolfram, 1983).

These computer models were first proposed by John von Neumann to study self reproducing systems (Von Neumann, Burks, et al., 1966) and has since been used to model pedestrian dynamics (Padovani, Neto, & Cereda, 2018), to predict environments subject to desertification (de Oliveira Barros et al., 2018), modeling crowd dynamics (Gerakakis et al., 2018), lava or mudflows (Vicari et al., 2007), and even more popularly in simple games like Conway's Game-of-Life.

The primary features of a cellular automaton are their state, their neighborhood, and the rule-set. A starting state is given to each cell and is expressed numerically, but depends on the property of interest and can be expressed as a binary variable or a non-binary variable (Arai, Basuki, & Harsono, 2012). For example a cell can be alive or dead (binary) or can have a certain porosity in a scale of 1% to 100%. The neighborhood consists on the surrounding cells of a specific cell. The two main neighborhood systems are the von-Neumann neighborhood and the Moore neighborhood (Arai et al., 2012) as seen in figure 2.7.

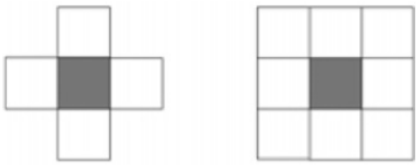

Figure (2.7) Neighborhood models for two-dimensional cellular automaton. Left: Von-Neumann, right: Moore. Adopted from (Arai et al., 2012).

2.2.2 Geological Applications

Geological models are traditionally presented in two-dimensional cross sections. Nowadays, these models are increasingly visualized as digital three dimensional models known through what is known as geomodelling (Apel, 2006). Generating computer based geological models has become increasingly popular as seen by the development of different software used in the mining industry (Leapfrog Geo, Maptek Vulcan, Dips, among others). Although the most conventional computer-based models used for geological purposes consist in 3D representations there are other ways in which computer algorithms have been proposed to aid in geological mapping and mining processes. Machine learning algorithms have been used to aid in mapping and in mineral prospectivity (Granek, 2016). The fact that machine learning algorithms are designed to identify and to predict patterns within multivariate data and can be efficiently applied to geoscience data obtained from field observations in order to further the understanding of the spatial distribution of complex geological phenomena (Cracknell, 2014).

Discrete computer models have also been applied to the mining industry including the study of granular flow in block caving (Miranda, 2017). This type of tool can be used for the extraction plan design at industrial scales. Mudflow prediction models have also been developed with discrete models. The LUSI mud plume at Sidoarjo, East Java was modeled with this type of computer model and showed relatively good prediction accuracy compared with conventional models (Arai et al., 2012). Even the lava flows of Mt. Etna have been modeled with MAGFLOW, a cellular automata based model, yielding consistent results except for the fact that ephemeral vent formations were not accounted for in the model (Vicari et al., 2007).

Chapter 3

Proposed Model

The model proposed in this study corresponds to a discrete model whose state is altered with time. This discrete dynamic model solves for variables analytically and numerically and the simulations are done based on equations obtained from literature or based on experiments found in literature.

3.1 Geological Model

The proposed geological model consists on an andesite host rock that is intruded by a magmatic fluid mixed with meteoric water. Both the host rock and the magmatic fluid have a defined chemistry. The global variables that this model focuses on are the fluid movement, the temperature interactions between the rock and the fluid, the depth at which the fluid and the rock interact and the pH of the fluid passing through the rock. These parameters were chosen considering Corbett & Leach (1998), which postulates that each hydrothermal alteration has a specific temperature, pH and depth range as seen in the previous chapter in figure 2.5. It is very important to highlight the fact that for the purposes of this study the fluid in question will be strictly in the liquid phase.

The aim for this model is to break up the different variables that influence the formation and emplacement of hydrothermal alterations and establish relationships for their change over time. The interactions that will be assessed in the subsequent simulations will be:

- Thermal exchange between the fluid and the host rock
- Flow of the fluid through a porous rock medium
- pH variation of the fluid while it flows through the rock medium
- The effect of the fluid on the host rock due to the interaction between the two

Table (3.1) Composition of the magmatic fluid used for this model, based on the fluid used in Reed ((1997)).

Magmatic condensate mixed with pure water				
Model Fluid Composition				
Component		m		ppm
Cl^-		0.403		13643
SO_4^{2-}		0.217		19955
HCO_3^-		0.16		9272
HS^-		0.00885		280
SiO_2		0.000545		31.1
Al^{3+}		0.177×10^{-5}		0.0457
Ca^{2+}		0.302×10^{-5}		0.116
Mg^{2+}		0.315×10^{-6}		0.00733
Fe^{2+}		0.105×10^{-4}		0.561
K^+		0.571×10^{-4}		2.14
Na^+		0.920×10^{-4}		0.0586
Mn^{2+}		0.112×10^{-6}		0.263
Zn^{2+}		0.420×10^{-5}		0.275
Cu^+		0.453×10^{-6}		0.312
Pb^{2+}		0.158×10^{-5}		0.677×10^{-5}
Ag^+		0.657×10^{-10}		0.168×10^{-4}
Au^+		0.657×10^{-10}		0.00387
Hg^{2+}		0.118×10^{-7}		0.000241
Ba^{2+}		0.184×10^{-8}		0.783
$Sb(OH)_3$		0.250×10^{-6}		0.0412
H_3AsO_3		0.650×10^{-5}		0.783

In order to achieve this, a rock grid is set up with specific initial states including rock density, porosity, temperature, thermal constants, composition and parameter defined as neutralization potential which will account for the host rock's ability to neutralize an acidic hydrothermal fluid. Likewise, the fluid will have a specific composition, thermal constants, temperature, density, viscosity, pressure and volume. Furthermore, the scale of the model is to be considered 5[km] x 5[km], scale obtained from Sillitoe (2010) 2.4.

For convenience and consistency the chemical compositions of the both andesite and fluid will be the ones used on Reed (1997). These compositions are found in tables 3.1 and 3.2. Host rock and fluid will interact to yield the change over time of the described variables. The equations governing the variations of these items will be described further ahead.

Table (3.2) Bulk composition of the andesite used for this model, based on the rock sample used in (Reed, 1997).

Bulk Rock Composition for Andesite used in the Model				
Compund		wt %	ppm	ppb
SiO_2		59.07		
Al_2O_3		17.43		
Fe_2O_3		2.56		
FeO		4.05		
MnO		0.12		
MgO		3.35		
CaO		6.77		
Na_2O		3.93		
K_2O		1.48		
BaO		0.0692		
NaCl		0.033		
H_2O		N/A		
CO_2		N/A		
S			200	
Cu_2O			48	
PbO			8.2	
ZnO			97	
Sb_2O_3			0.24	
As_2O_3			3.3	
Au				4
Ag				80
Hg				10

3.2 Computational Conceptualization

The computer model is a discrete model based on cellular automata. This model consists on a 2D grid representation of the spatial zoning of a porphyry copper deposit. To achieve this, there is a discretization of space in this model represented in square grids. Therefore, there are two important components to be taken into account, the host rock and the hydrothermal fluid that flows through this rock. The host rock will be represented by a grid consisting of square cells. Each square cell has an initial state which will be altered in time when it interacts with fluid. The fluid will consist on its own grid with its own initialization parameters. There is also another type of fluid grid which slightly varies in concept with respect to the previous two grids. This new fluid grid consists in the information storage of a new incoming fluid. In other words, this grid sets where the fluid flux will be first present, the magnitude of this flux and some other initial parameters of the fluid.

The initial states of each grid are altered when the two grids interact. In order to interact, these two grids must have the same square geometry and the same dimensions. These interactions are calculated when the index of a cell within the fluid grid matches the index of a rock grid. The interactions will be calculated at each cell. Old parameters will enter an algorithm and new values for the same variables will be the output. With each iteration the cells will be updated as seen in figure 3.1.

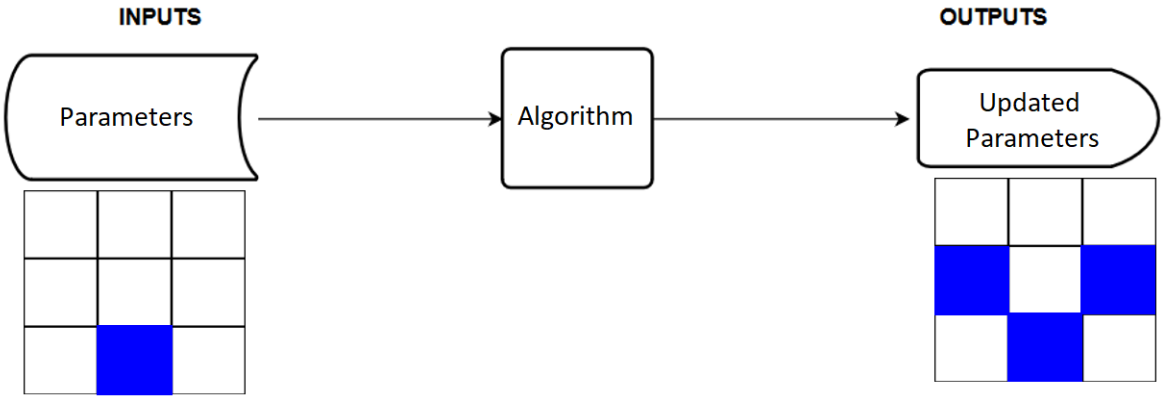

Figure (3.1) Schematic representation of how the grids' parameters are updatedt.

3.2.1 Methodology and Structure

The algorithm proposed in this work follows a simple architecture. Following the development of a conceptual model of a subsurface domain, the simulations follow a certain course of action. This workflow includes a pre-processing step. At this stage the model geometry is defined including the rock grid and the fluid grids. The variables that each grid contains is also defined in this step, but not set to a specific value. This is more of a specification of what attributes the grids will have. For example, the rock grid has a specific density, temperature, porosity and thermal constants.

Following this pre-processing the parameters are initialized. Starting values are assigned to the parameters. This includes physical parameters such as gravity, specific heats of rock and fluid, viscosity coefficients, constants for different interactions and porosity ranges for the rock. The values for the cell sizes in equivalence to real-life dimensions are specified, as well as their neutralization potential and temperature ranges based on a geothermal gradient. The fluid constants and starting parameters are also set at this stage. Starting temperatures, pH conditions, NaCl content, flux and temperature are specified and given numerical values. Other specifications like the time intervals, number of iteration and simulation constants such as decay factors are integrated into the model in this step.

The next step in this workflow are the interactions of the parameters. This step represents the main step of this project because it is at this step that the parameters will variate and yield results. The simulation of new parameters takes place at this step through the solving of specific equations acquired from the corresponding literature. These new parameters are stored at certain time intervals set in the initialization step until a specified end time is

achieved. In this step six main interactions are simulated and updated throughout the spam of the simulation. In other words, in order to obtain the final results, the values of these parameters are computed through iteration. These interactions are:

- Fluid movement
- Thermal exchange between rock and fluid
- Fluid viscosity variation
- Fluid density variation
- Rock porosity variation based on fluid pH
- Fluid pH variation

Following the rock–fluid interaction stage, the visualization of the results of said interactions is generated. In this step visual maps of the variation of desired variables is obtained. One can observe where the fluid moved, how its temperature changed, the pH of the fluid at certain points in time and consequently the hydrothermal alterations these variables describe. These visualizations yield exhibit the results of a simulation with specified parameters. A conceptual map of the entire code structure is seen in figure 3.2.

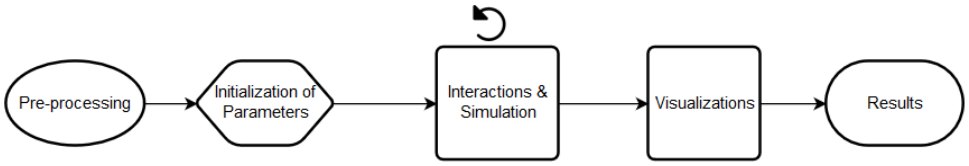

Figure (3.2) Overview of the structure followed in the code presented in this document. The recurring arrow indicates that this step is iterated over time.

3.2.2 Governing Equations

In this study a single-phase, non-isothermal flow of a fluid with a variable density flowing through a porous media is considered in order to study each interaction. Now each interaction will be broken down and exhibit what equation or set of equations govern the change of the parameters involved.

Fluid Movement

To study the movement of the fluid through a porous media, Darcy's law is used. Darcy's law describes how a liquid can move through a porous media (Bear, 2013). This equation can be expressed in vector form as:

$$q = -\frac{k}{\mu}(\nabla P - \rho g \hat{\boldsymbol{z}}) \tag{3.1}$$

Where:

- q is the discharge per unit area in $[\frac{m}{s}]$
- k is the permeability of the porous medium in $[m^2]$
- μ is the dynamic viscosity of the fluid in $[Pa \cdot s]$
- ∇P is the pressure gradient vector in $[\frac{Pa}{m}]$
- ρ is the density of the fluid in $[\frac{kg}{m^3}]$
- g is the acceleration due to gravity in $[\frac{m}{s^2}]$ which only affects the movement in the vertical component, hence the unit vector $\hat{\boldsymbol{z}}$

In this case gravity will not be accounted for in this model similarly to how it is done in Fowler et al. (2016) yielding the more simplified version of this equation:

$$q = -\frac{k}{\mu}\nabla P \tag{3.2}$$

Conservation of mass is expressed by the continuity equation utilized in Darcy's law, considering a 2D space:

$$0 = -\frac{k}{\mu}(\frac{\partial^2 P}{\partial x^2} + \frac{\partial^2 P}{\partial y^2}) \tag{3.3}$$

Assuming an isotropic medium where k is the same in $\hat{\boldsymbol{x}}$ as it in $\hat{\boldsymbol{y}}$ and taking into account a fluid source(W) and 3.3 can be expressed as:

$$0 = -\frac{k}{\mu}(\frac{\partial^2 P}{\partial x^2} + \frac{\partial^2 P}{\partial y^2}) + W \tag{3.4}$$

Which can be simplified to:

$$0 = -\frac{k}{\mu}\nabla^2 P + W \tag{3.5}$$

Equation 3.5 represents the steady state flow of a fluid through a porous media. In the next chapter the implementation of this equation will be explained together with how this Poisson equation is solved.

Fluid Viscosity

It is relevant to mention that for simplification the viscosity of a hydrothermal fluid will be obtained by using the viscosity of water at various temperatures. Obtaining the fluid dynamic viscosity is necessary in order to use equation 3.5. Viscosity is friction within a fluid that results from the strength of molecule to molecule attractions. This resistance to internal shear causes a fluid to resist flow through geologic materials. The viscosity of a liquid generally decreases with increasing temperature, including aqueous solutions (Fitts, 2013).

To calculate the variation of viscosity with temperature an Arrhenius model of viscosity (seen in equation3.6) is presented.

$$\mu = \mu_0 \mathrm{e}^{\frac{E_a}{RT}} \tag{3.6}$$

Where:

- μ is the dynamic viscosity of the fluid in $[Pa \cdot s]$
- μ_0 is a pre-exponential factor in $[Pa \cdot s]$
- E_a is the activation energy for viscous flow in $[\frac{J}{mol}]$
- R is the gas constant which it is equivalent to $8.314[\frac{J}{K \cdot mol}]$
- T is the temperature of the fluid in Kelvins [K]

Table (3.3) Viscosity of water at various temperatures. Adopted from (Korson et al., 1969).

Viscosity (mPa s)	T(C°)	T(K)	1/T[1/K]
1.7916	0	273	0.003663
1.5192	5	278	0.003597
1.3069	10	283	0.003534
1.1382	15	288	0.003472
1.002	20	293	0.003413
0.8903	25	298	0.003356
0.7975	30	303	0.0033
0.7195	35	308	0.003247
0.6532	40	313	0.003195
0.5963	45	318	0.003145
0.5471	50	323	0.003096
0.5042	55	328	0.003049
0.4666	60	333	0.003003
0.4334	65	338	0.002959
0.4039	70	343	0.002915
0.3775	75	348	0.002874
0.3538	80	353	0.002833
0.3323	85	358	0.002793
0.3128	90	363	0.002755
0.2949	95	368	0.002717
0.2783	100	373	0.002681

It is important to notice that there are two constants that are yet unknown. These constants are E_a and μ_0. There is a methodology to be followed in order to find these two parameters. Following the methodology of Tunick (2010) and Scarfe & Cronin (1986), E_a is proportional to the slope of the line in the Arrhenius plot of $\ln \mu$ versus $\frac{1}{T}$. Taking the values found in Korson et al. (1969) seen in table 3.3 and plotting them into a scatter plot, one can add a linear trend-line to the data and obtain a value for the E_a as seen in figure 3.3.

With the value for E_a obtained (1852.4 $\frac{J}{K \cdot mol}$) it is possible to obtain the value for μ_0 by using equation 3.6, using the value of density at a specific temperature from table 3.3 (in this work the values at 298 K were used) and solving for μ_0. Through this method an approximated value of $0.000421[Pa \cdot s]$ is obtained for μ_0.

Thermal Exchange

Taking into account only conduction in which thermal energy exchange is due to exchange of kinetic energy among colliding molecules without displacement, the main two relationships used to study the change of temperature in the host rock as well as in the hydrothermal fluid are Newton's cooling law and Fourier's law seen in equations 3.7 and 3.8 respectively.

$$\frac{J_t}{A} \approx -h(T - T_0) = \frac{\mathrm{d}T}{\mathrm{d}t} (Besson,2012) \tag{3.7}$$

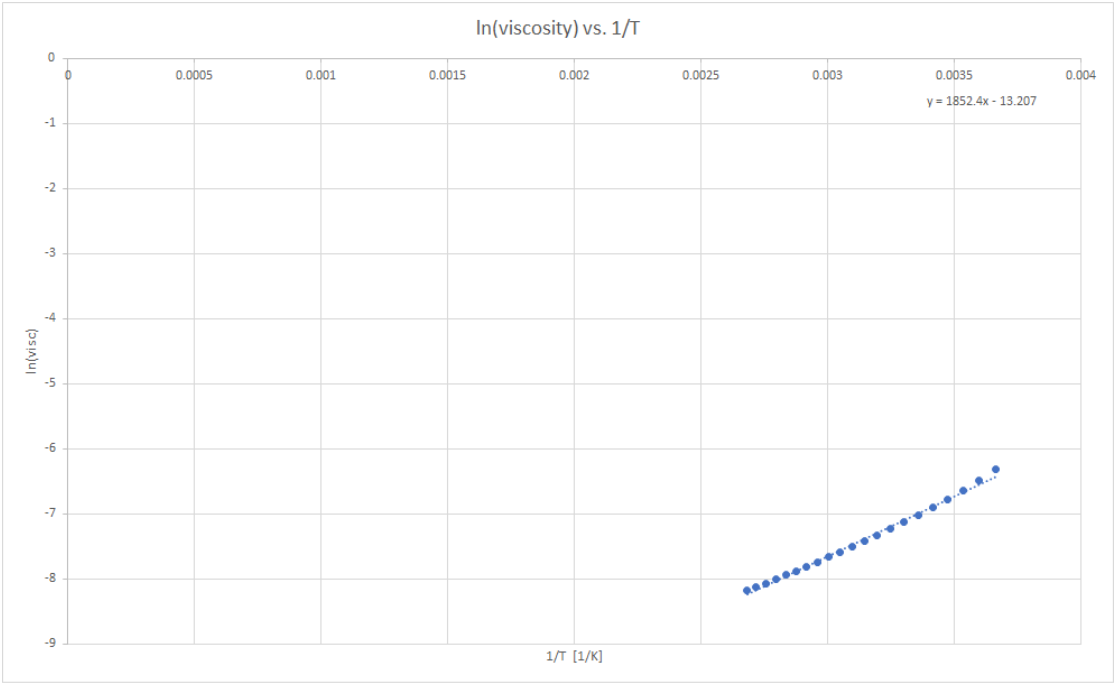

Figure (3.3) $\ln(viscosity)$ vs. $\frac{1}{T}$ based on the data seen in 3.3. The slope in the obtained trend-line yields the value for E_a.

Where:

- J_t is the rate of heat transfer in $[W]$
- $\frac{\mathrm{d}T}{\mathrm{d}t}$ is the change of temperature with time $[\frac{K}{s}]$
- h is the heat transfer coefficient in $[\frac{W}{m^2 \cdot K}]$
- T_0 is the initial temperature of the fluid in Kelvins [K]
- T is the temperature of the fluid at a point in time in Kelvins [K]
- A is the area of the flow in $[m^2]$

$$\frac{J_h}{A} = -\frac{\lambda \nabla T}{L} \tag{3.8}$$

Where:

- J_h is the conductive heat flow rate in $[W]$
- λ is the thermal conductivity or heat conductivity of a certain material in $[\frac{W}{m \cdot K}]$
- ∇T is the temperature gradient vector in $[\frac{K}{m}]$

According to Robertson (1988), when considering only conduction the following relationship between h and λ can be written equating Fourier's law 3.8 to Newton's law of cooling 3.7 :

$$\frac{J_h}{A} = -h(T - T_0) = -\lambda(T - T_0) \tag{3.9}$$

Therefore,

$$L = \frac{\lambda}{h} \tag{3.10}$$

Where L represents the thickness of the medium in [m].

In order to maintain a conservation of heat the zeroth law of thermodynamics (equation 3.11) is used. This relationship quantifies the heat transfer between two medias, in this case the host rock and the fluid.

$$Q = m \cdot c\Delta T \tag{3.11}$$

Where:

- Q is the heat energy in [J]
- m is mass of the medium in [kg]
- c is the specific heat of the medium in $[\frac{J}{kg \cdot K}]$
- ΔT is the change in temperature in the medium in [K]

In order to conserve the heat lost by one media (fluid) and gained by the other (host rock) the following equation will be established 3.12:

$$Q_r = -Q_f \tag{3.12}$$

Where:

- Q_r is the heat energy gained by the rock in [J]
- Q_f is the heat energy lost by the hydrothermal fluid in [J]

Replacing equation 3.11 in equation 3.12 it is possible to obtain the temperature change in the two media.

Fourier's law can also be expressed in differential form in terms of the temperature variation trough time as seen in equations 3.13 and 3.14.

$$\frac{\mathrm{d}T}{\mathrm{d}t} = \alpha \nabla^2 T \tag{3.13}$$

Where:

$$\alpha = \frac{\lambda}{\rho \cdot c} \tag{3.14}$$

- $\frac{\mathrm{d}T}{\mathrm{d}t}$ is the temperature variation with time in $[\frac{T}{s}]$
- α is the thermal diffusivity of a specific medium in $[\frac{m^2}{s}]$
- ρ is the density of the medium $[\frac{kg}{m^3}]$
- $\nabla^2 T$ is the net temperature transfer per area in $[\frac{K}{m^2}]$
- c is the specific heat of the medium

This final equation is also a Poisson equation similar to that of the fluid movement (equation 3.5). These two expressions will be solved in an almost identical fashion. Furthermore, it is relevant to mention that for simplification constant values for the thermal conductivity will not vary with temperature or pressure.

Fluid Density

In order to calculate thermal diffusivity the density of the fluid is needed. The hydrothermal fluid in this case will be treated as brine, that is an NaCl aqueous solution as salt content has a great impact on this parameter (Potter & Brown, 1975). This is because finding the density of an aqueous solution can be very complicated that has dedicated entire research topics to find densities in very specific temperature and pressure intervals.

For simplification, the relationship proposed (equations 3.15, 3.16 and 3.17) in Haas (1971) is used to calculate the density of a saline hydrothermal fluid. This equation has a precision of 0.002 $\frac{g}{cm^3}$ in a temperature range of 75°to 325°C.

$$\rho = \frac{1000 + Mx}{1000V_0 + \phi x} \tag{3.15}$$

Where:

- ρ is the density of the fluid in $[\frac{g}{cm^3}]$
- M is the molecular weight of NaCl in $[\frac{g}{mol}]$
- V_0 is the specific volume in $[\frac{cm[3}{gH_2O}]$
- ϕ is the apparent molal volume of NaCl in aqueous NaCl in $[\frac{cm^3}{moleNaCl}]$
- x is the concentration of NaCl in molal units $[\frac{mole}{1000g}]$

$$V_0 = \frac{V_c + a_1\theta^{\frac{1}{3}} + a_2\theta + a_3\theta^4}{1 + a_4\theta^{\frac{1}{3}} + a_5\theta} \tag{3.16}$$

Where:

- θ = 647.27 - T_x
- T_x = temperature of the brine (fluid) in [K]
- V_c = 3.1975
- a_1 = -0.3151548
- a_2 = -1.203374 $\cdot 10^{-3}$
- a_3 = 7.48908 $\cdot 10^{-13}$
- a_4 = 0.1342489
- a_5 = -3.946263 $\cdot 10^{-3}$

$$\phi = b_0 + b_1 V_0 + b_2 V_0^2 + x^{\frac{1}{2}}(b_3 + b_4 V_0)(\frac{V_c}{V_c - V_0})^2 \tag{3.17}$$

Where:

- b_0 = -167.219
- b_1 = 488.55
- b_2 = -261.07
- b_3 = -19.644
- b_4 = 13.97

To calculate the density of the saline solution outside the temperature range mentioned before (75°to 325°C) the following exponential decay function is used:

$$A \cdot \mathrm{e}^{-\xi \cdot (T_f - T_{maxbrine})} + \rho_{min} \tag{3.18}$$

Where:

- A is the density of the fluid at the maximum temperature (598 [K]) where equation 3.15 is valid
- ξ = is a decay constant determined during simulation tests with a value of 0.001
- T_f = current temperature of the fluid in [K]
- $T_{maxbrine}$ is the maximum temperature (598 [K]) where equation 3.15 is valid
- ρ_{min} is an approximation of the minimum density a liquid saline solution could achieve before turning into a super-critical fluid. In this case this is considered to be 300 $[\frac{kg}{m^3}]$ (García, Pérez, Fdez-Polanco, & Cocero, 2003)

In this fashion, an approximation of how the density of the hydrothermal fluid behaves at high temperatures.

Porosity and pH Variations

The interaction between rock and hydrothermal fluid has effects on the pH of the fluid because of the acid neutralization by wall-rock reaction. Aqueous H^+ ions are consumed in exchange for cations from the rock. This acid neutralization is due to mineral pH buffer series (Smith et al., 2017). At the same time, the consumption of these mineral buffers alter the original porosity of the host rock. The pH and porosity variation is due to the water/rock ratio. The pH will increase as the water/rock ratio increases and the same happens with the rock porosity. (Reed, 1997). To model this, the experimental curves obtained from Reed (1997) and Smith et al. (2017) are used (seen in figures 3.4 and 3.5). These experiments were done using the compositions seen in tables 3.2 and 3.1

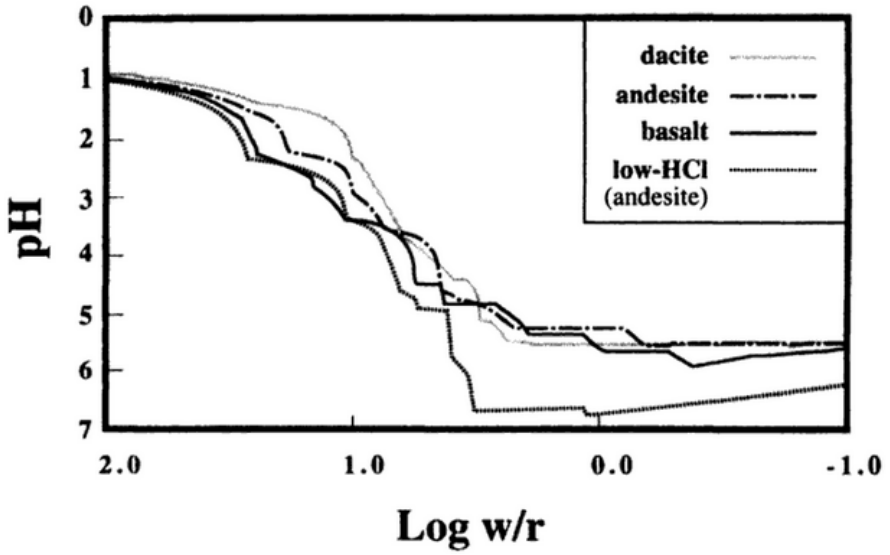

Figure (3.4) pH as a function of $\log(w/r)$ for the reaction of different rock types with a hydrothermal fluid, adopted from (Reed, 1997)

Based on these experimental curves it is possible to acquire a relationship between water/rock ratio and the pH variation of a fluid. A polynomial trend line is obtained from Reed (1997) data which yields the equation:

$$pH = 0.1667x^3 - 0.5x^2 - 1.6667x + 5.5 \tag{3.19}$$

Where x is the $\log(water/rock)$.

The problem with this interaction is the fact that it is defined for an input of a fluid pH of around 1. To take into account the fact that not always the input fluid is 1 a linear interpolation is made to address other input pH. To account for the fact that the buffer minerals will be consumed in time, an exponential function is applied to decrease the effect of neutralization by the rock.

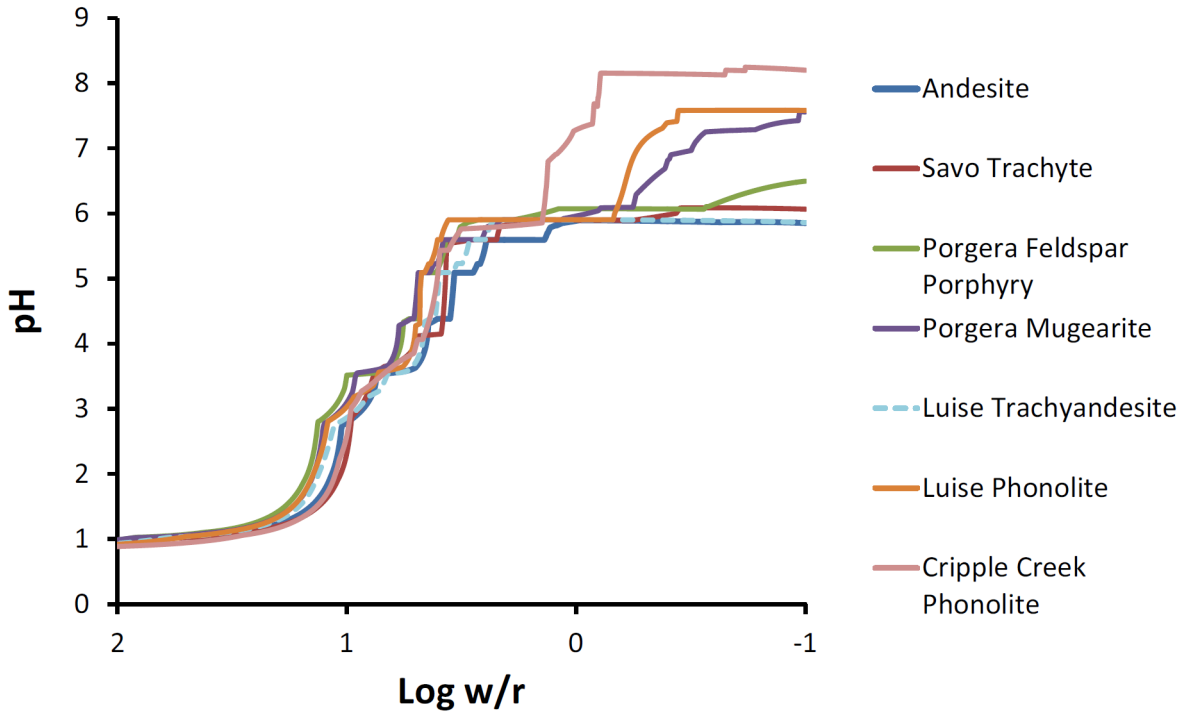

Figure (3.5) Increasing pH as a result of decreasing water/rock ratio, adopted from (Smith et al., 2017)

The linear interpolation obeys the following relationship:

$$pH_{new} = pH_{input} \cdot m + b \tag{3.20}$$

Where:

- pH_{new} is the resulting pH without taking into account the neutralization potential of the rock
- pH_{input} is the current pH of the fluid
- m is the slope of the linear interpolation given by:

$$m = \frac{7 - pH_{\text{reed}}}{6} \tag{3.21}$$

- pH_{reed} is the pH obtained from the interaction in equation 3.19
- $b = pH_{\text{reed}} - m$

The exponential decay of the neutralization potential of the rock is given by:

$$NP = B \cdot \mathrm{e}^{-\chi \cdot NP_{input}} \tag{3.22}$$

Where:

- NP is the resulting neutralization potential of the rock
- $B = pH_{input} - pH_{new}$
- χ is a decay factor with an arbitrary value of 10^{10}
- NP_{input} is the intact neutralization potential

Using 3.20 and 3.22 yields the final relationship for the resulting pH:

$$pH = pH_{input} - NP \tag{3.23}$$

The new porosity is obtained using a linear interpolation model of pH_{input}, an exponential decay of water/rock ratio and an exponential decay of neutralization potential given by:

$$\Phi = \Phi_{new} - (\Phi_{new} - \Phi_{in}) \cdot e^{-\kappa \cdot x \cdot NP} \tag{3.24}$$

Where:

- Φ is the resulting porosity of a rock cell after interacting with a given fluid
- Φ_{new} is the interpolated value of porosity acquired from

$$\Phi_{new} = pH_{input} \cdot m_{por} + b_{por} \tag{3.25}$$

- m_{por} is the slope of the linear interpolation $= \frac{\Phi in - \Phi_{max}}{6}$
- Φ_{in} is the current porosity of a rock cell
- Φ_{max} is a maximum porosity that a rock cell could achieve based on (Reed, 1997), a value of 0.43
- pH_{input} is the current pH of the fluid
- κ is a decay factor with an arbitrary value of 10^{10}
- NP_{input} is the intact neutralization potential

Overall, these are the equations that will govern the interactions in the computational model proposed.

Chapter 4

Implementation

4.1 Programming Language and Design

In order to implement the proposed model it is necessary to chose a programming language. The chosen language is Python 3. According to Python Software Foundation, Python is an interpreted, interactive, object oriented programming language that combines remarkable power with very clear syntax in addition to being extensible in C or C++ and being portable to different operating systems (*General Python FAQ*, n.d.). In general, Python is a high level general purpose language that comes with a large standard library including HTTP, FTP, SMTP, XML-RPC, POP, IMAP and CGI programming.

Python was first released in 1991 by its developer Guido van Rossum who sought to create a simplified programming language (*General Python FAQ*, n.d.) The legibility, simplicity, applicability and object oriented factors of this programming language made it ideal for the purpose of this study.

In terms of integrated development environment or IDE, PyCharm was the preferred on to work on this project. The intelligent assistance such as code completion, inspections, error highlighting and fixes makes a friendly and simple work environment. Furthermore, PyCharm supports Anaconda as well as scientific packages like matplotlib, NumPy and SciPy which were utilized in this project. Most importantly the built in tools like debugger and integrated terminal makes code testing much faster and efficient.

Given the object oriented language chosen to accomplish this work, the computational model proposed to simulate this phenomena follows this approach. Object oriented programming consists on a set of objects that can vary dynamically and can be executed by acting and reacting to each other. The goal of an object oriented analysis is to define classes, the relationships and behavior associated with them that are relevant to the solution of a problem. This allows the separation of a program into a network of subsystems that independently control their own data and algorithms (Asagba & Ogheneovo, 2008). Objects are instances of a class, each object has the behaviors of its class. This retroactively means that a class describes the contents of the objects that belong to it. A class describes an aggregate of

data fields (instance variables) and defines its functions (methods). A method is simply an action which an object is able to perform (Chailloux, Manoury, & Pagano, 2007). Object oriented programming exhibits a series of properties that are mainly characterized by (Asagba & Ogheneovo, 2008):

- Data Abstraction: Methodology that enables the isolation of a compound data objects that pertain to a class without entering in complex specification of how they are implemented.
- Encapsulation: Ability to package codes and data together in a single place, preventing access to them by any other means different from the previously specified ones.
- Polymorphism: Mechanism that allows different objects to respond differently to the same function call.
- Inheritance: Ability of an existing class to create new classes. Existing classes are referred to as base classes and the offspring classes are called derived classes. This allows program reuse, reliability and modification of base classes.

These concepts and characteristics make object oriented programming a good fit for achieving the goal of this work. The model proposed in this work consists on the definition of classes, the initialization of their variables, the specification of their methods, the visualization of the variables and the general output of the algorithms.

4.2 Defining Objects

The primary class used in this work is the Grid class. This class consists on generating a grid of n blocks by n blocks, parameters, and other matrix data. The methods associated to this class are a method to obtain a variable and another to over-write a variable.

Three derived classes are inherited from the primary Grid class. First of whom is the RockGrid class which stores the information of the host rock variables. In addition to the parameters and methods of the regular Grid class, RockGrid specifies the parameters that it contains, specifically a neutralization potential, porosity, temperature, a dictionary of values used in the simulation and the number of rock cells (blocks). One of the new methods defined in this derived class is the *get_void_volume* method which obtains the volume of the pores through the simple relationship:

$$pore\_volume = porosity \cdot volume\_of a\_rock\_cell \tag{4.1}$$

Another method utilized in this class is the *get_lithostatic_press* method which based on the rock density, gravity and depth of the rock cell yields the lithostatic pressure on that cell.

The block size, rock density and gravity are parameters that require initialization and are saved under parameters associated to the objects. Other classes described in this excerpt also have parameters that require initialization. Initializations will be discussed further ahead.

Another derived class from the Grid class is the FluidGrid class which stores the information of the fluid variables and representation. FluidGrid requires a dictionary of NumPy matrices with the same dimensions whose key values are:

- Fluid Density
- NaCl content in the fluid
- Initial pH of the fluid
- Pressure of the fluid
- Initial Temperature of the fluid
- The incoming fluid Volume

These parameters are saved under matrix data and in addition to this the FluidGrid requires a dictionary of values used in the simulation and a tuple with the dimensions of the model. The new methods associated with this class are the *get_fluid_presence* method which returns whether or not there is fluid in a cell based on if there is fluid pressure on that cell. The other method associated with this class is the *get_viscosity* method which uses equation 3.6 to compute the viscosity of the fluid at a given cell under certain conditions.

The final Grid derived class is the RecordedFluid class which records the information of the fluid associated to hydrothermal alterations and the simulation parameters such when the simulation stops. The matrix data necessary for this class are:

- pH of the fluid at a certain point in time in the simulation
- Temperature of the fluid at a certain point in time in the simulation
- Water/Rock ratio

This class also needs a dictionary of values used in the simulation as well as the dimensions of the model. The methods defined in this class are the *get_depth* method which returns the depth at which the fluid was present and the *update_water_rock_ratio* method which updates the water/rock ratio of a cell based on the volume of fluid in the cell and the porosity of the cell block interacting with it.

Another base class defined in this model is the IncomingFluidGrid class which stores the information of a fluid that is about to enter the interaction vicinity of a rock grid. In other words this class represents a fluid that is about to enter the n by n blocks model that has been previously defined. This class has a method which verifies that the incoming fluid is within the range of the cell model. This is because the incoming fluid will be entering at a certain column in the model. This method asserts that the incoming fluid is in a valid column position. Another important method in this class returns the fluid flux, the column in which the fluid will be injected, the temperature, pH, NaCl content and the density of the incoming fluid.

The base class IterativeModel creates objects whose purpose is to set simulation times based on parameters obtained from grid objects, to run the model and to analyze if the simulation is running on an already altered model, that is to say a host rock that has already interacted with a previous fluid. This class is the parent class of perhaps the most important class in this project, the Interactions class. This class defines all the interactions further explained in section 4.4 in addition to a method that saves images of the parameters' states during the simulation, another method that updates the pH, temperature and water/rock ratio with obtained values from the interactions and finally a method that generates the visual representations of hydrothermal alterations in an RGB color scale.

Overall, the relationships among classes are illustrated in figure 4.1.

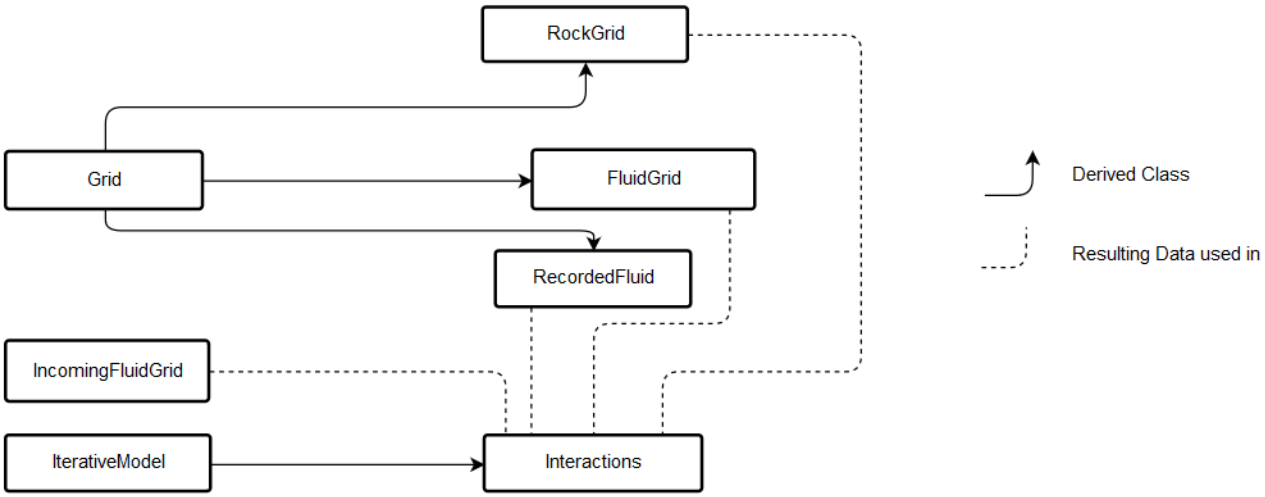

Figure (4.1) Diagram of existing classes in the proposed model and how they relate and interact with each other

A further explanation on how the variables are initialized and how each interaction is implemented and computed is specified in the following sections.

4.3 Initialization of Variables

Initializations are not defined as classes but rather as stand-alone functions, more correctly referred to as user-defined functions. A function is a block of organized, reusable code that is used to perform a single action. In this project initializations are stored in their own folder, where their values can be easily accessed and edited. These values are organized into the following eight categories:

- Physical Parameters
- Fixed Simulation Parameters
- Rock Grid Initialization
- Fluid Grid Initialization
- Recorded Fluid Grid Initialization
- Number of Iterations

Some initialization functions do not set a value, but create the dictionary for the values so that a user may specify them during a run of the program. The ultimate purpose of the initializations is to set up the necessary values and/or parameters that the objects need to execute their methods.

4.3.1 Physical Parameters

This section specifies initial physical values of the fluid, the rock and also the gravity. For simplification gravity is considered a constant in this model. The physical parameters consist of:

- Gravity g = 9.8 $[\frac{m}{s^2}]$
- Rock Specific Heat c_r $[\frac{J}{kg \cdot K}]$ from (Eppelbaum, Kutasov, & Pilchin, 2014)
- Density of Rock $\rho_r = 2600$ $[\frac{kg}{m^3}]$ from (Klein & Johnson, 1983)
- Fluid Specific Heat $c_f = 4184$ $[\frac{J}{kg \cdot K}]$ from (Perlman, 2018)
- Activation Energy for viscous flow $E_a = 1852.4[\frac{J}{K \cdot mol}]$ from 3.3
- Universal Gas Constant R = 8.314 $[\frac{J}{K \cdot mol}]$
- Thermal Conductivity of Andesite $\lambda_r = 2.26$ $[\frac{W}{m \cdot K}]$ from (Sharma, 2002)
- Thermal Conductivity of water at $20°C$, $\lambda_f = 0.6$ $[\frac{W}{m \cdot K}]$ from (Eppelbaum et al., 2014)
- Maximum Rock Porosity $\Phi_{max} = 0.43$ based on (Reed, 1997)
- Minimum Fluid Density = 300 $\rho_{f_{min}}$ $[\frac{kg}{m^3}]$ from (García et al., 2003)

These parameters are then saved into dictionaries associated with the rock grid, fluid grid, or global parameters. It is important to mention that for simplification the thermal conductivity of the fluid is considered to be the λ_f and is a constant value as well as $\lambda - r$.

4.3.2 Fixed Simulation Parameters

The parameters initialized in this section correspond to non variable values used in the simulation such as decay factors which have been specified in section 3. An important parameter defined here is the porosity to permeability factor. Equations 3.1, 3.2, 3.3, 3.4 and 3.5 utilize the permeability of the medium, but the change of porosity of the rock changes the permeability of the medium. Using a capillary tube model for the rock's porosity the porosity-permeability relationship can be defined as:

$$k = \frac{\Phi \cdot r^2}{8 \cdot \tau} \tag{4.2}$$

Where:

- k is the permeability of the porous medium in $[m^2]$
- Φ is the porosity
- r is the radius of the capillary tube in [m]
- τ is the hydraulic tortuosity

Hydraulic tortuosity is a dimensionless parameter that quantifies the non-straight streamline of a fluid in a porous medium, which in a wide range of porosities it can be considered to be approximately equal to $\sqrt{\frac{5}{2}}$ (Matyka, Khalili, & Koza, 2008). For simplification this value of tortuosity is considered constant in this model.

4.3.3 Rock Grid Initialization

To initialize the rock grid, a function is defined that calls upon the neutralization potential counter of each rock cell in a rock grid, the porosity tendency of the rock grid (from Reed (1997)) a standard of 25% to 30% initial porosity of a fractured andesite is derived), the thermal range of the rock grid associated with a geothermal gradient (with a mean of $49.35\frac{^\circ C}{km}$) which is the average gradient in the Chilean Andes (Muñoz & Hamza, 1993). These parameters are then stored in a dictionary containing the grid's data.

4.3.4 Hydrothermal Fluid Grid

The Hydrothermal fluid grid is initialized similarly to the rock grid only differing in the parameters that are initialized. The initialized and subsequently stored parameters associated to the fluid are:

- Initial fluid density obtained from equations 3.15 and/or 3.18
- NaCl content within the range of 7.3 molal
- Initial fluid pH (equal to 1 considering Reed (1997)'s data)

- Initial fluid temperature
- Volume of fluid injected

4.3.5 Recorded Fluid Grid

The recorded fluid grid is the grid that saves the pH, temperature, water/rock ratio, and position of the injected fluid in relation to the rock cells it interacted with.This data is used to generate the alteration zoning of the simulated porphyry copper deposit. Following the methodology used for the initialization of the two previous grids, the aforementioned parameters are saved into a dictionary.

4.3.6 Number of Iterations

In this initialization the time intervals for each iteration and the stabilizing time for each simulation are associated with a dictionary key to be later specified during test runs or simulation runs. The initialization function acquires these parameters and returns the overall time of each run. These simulation parameters can be changed for each run.

4.4 Interactions

The Interactions class has various methods that are the core of the simulation model proposed in this project. These methods update the initial and intermediate states of the rock grid as well as the fluid grid. It is important to keep in mind that the Interactions class is a derived class from the IterativeModel class. The methods that govern the phenomena modeled in this algorithm are:

- fluid_movement
- thermal_exchange
- update_fluid_density
- update_porosity_ph
- save_image_status
- update_recorded_fluid
- post_processing

Overall, these methods are responsible for how the fluid interacts with its host rock. The outcome of these methods show the simulated spatial distribution of the alteration zones on the rock grid.

4.4.1 Fluid Movement

The main purpose of the method *fluid_ movement* is to utilize equation 3.5 to dictate where a fluid cell will move next. In order to accomplish this task the method needs the position of the fluid, permeability of the rock grid at that position and of its neighbors, the viscosity of the fluid and the pressure of the fluid. Since equation 3.5 is a Poisson equation, it is necessary to solve it before an output is obtained.

The method is organized into four stages. The first one consists on acquiring the input parameters specified before. At this stage the fluid viscosity is computed which is further described at the end of this section.

The second stage is to calculate the harmonic means of the porosity between transitions of a cell and its four neighbors (up, down, left, right). Since the cells at the borders do not have four neighbors a padding of the fluid grid is done. This padding consists on adding an extra row at the top and bottom of the grid and an extra column at the left and right of the grid. These new columns and rows have the same parameters of their adjacent neighbors.

Finally the iterative Poisson solver is computed in order to perform Darcy with fluid continuity. This consists on using the harmonic mean of the permeability between a rock cell and its neighbors, as well as the mean viscosity of the fluid. Then an iterative Poisson solver is computed for equation 3.5. This solver consists on using the mean permeability obtained in the previous step and compute the pressure gradient associated with the fluid so that the following relationship is established:

$$P = \frac{1}{\sum k_{mean_{neigh}}}((\sum P_{neigh} \cdot k_{mean_{neigh}}) + W) \tag{4.3}$$

Where:

- P is the pressure gradient
- $k_{mean_{neigh}}$ corresponds to the harmonic mean of the permeability between the current cell and one of its neighbors. The sum of these terms translates into the sum of the means between the current cell and each of its neighbors (up, down, left right)
- P_{neigh} is the pressure between the current cell and one of its neighbors
- W is a fluid source

The outcomes of these computations are a new position for the fluid, an outgoing pressure, and an outgoing discharge based on this pressure. The method also assigns all of the fluid parameters to the new position. This includes, density, NaCl content, pH, temperature and viscosity. It is important to keep in mind that the permeability is obtained from equation 4.2.

The overall functionality of this method can be summarized in figure 4.2

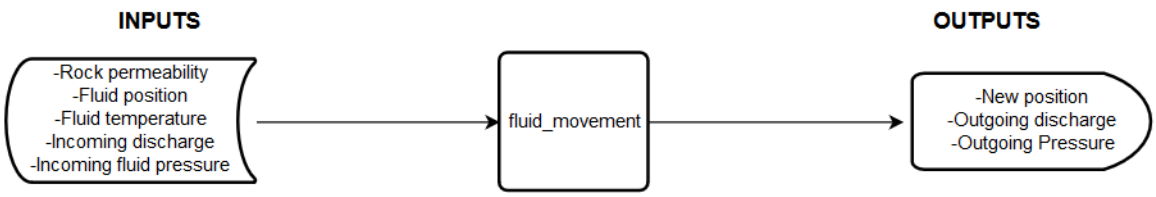

Figure (4.2) Schematic representation of the *fluid_movement* method in the Interactions class.

Fluid Viscosity

The fluid viscosity is computed within this method using equation 3.6. This is the reason why the temperature of the fluid is a required input in this method. The input parameters needed to compute this are the temperature of the fluid together with the constants for activation energy and the universal gas constant. Without the viscosity the first factor in equation 3.5 cannot be acquired.

4.4.2 Thermal Equilibrium

The *thermal_exchange* method in the Interactions class basically takes the temperature of the rock and the temperature of the fluid at a certain position and updates the temperature of both rock and fluid. To complete this task the method takes as inputs the position of the fluid, the volume, specific heat, density, thermal conductivity and temperature of the fluid at that position as well as the specific heat, volume, density, temperature and thermal conductivity of the rock at the position where the fluid is present. A schematic representation of the inputs and outputs of the *thermal_exchange* method can be observed in figure 4.3.

The *thermal_exchange* method takes a three step process to yield the temperatures of the rock and the fluid at a given position. First it uses equation 3.11 to compute an intermediate temperature between the rock and the fluid. Then this intermediate temperature is used to calculate a new temperature for the fluid through solving the differential equation 3.7. With this temperature using again 3.11 it is possible to obtain the new temperature of the rock cell. Finally, similarly to the fluid movement methodology, an iterative Poisson solver is computed to guarantee a continuity in the heat flow.

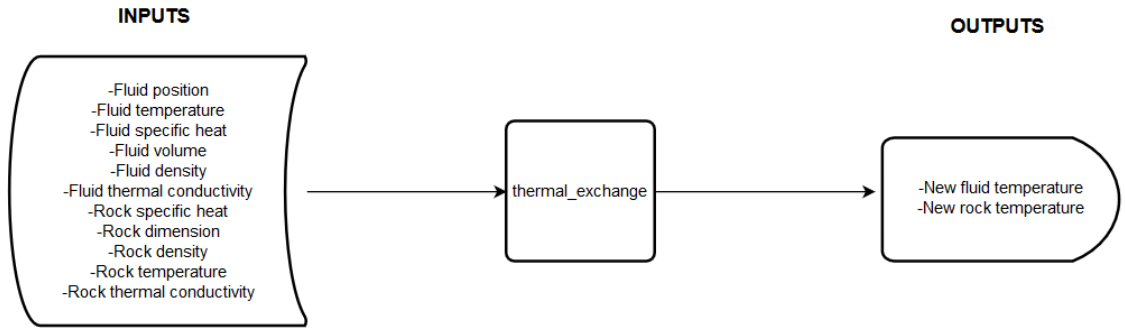

Figure (4.3) Schematic representation of the *thermal_exchange* method in the Interactions class.

4.4.3 Fluid Density

The fluid's density is updated through the *update_fluid_density* method in the Interactions class. Using equations 3.15 and 3.18. As seen in figure 4.4, the method takes as inputs the temperature of the fluid and NaCl content in the fluid. The method yields a new density for the fluid.

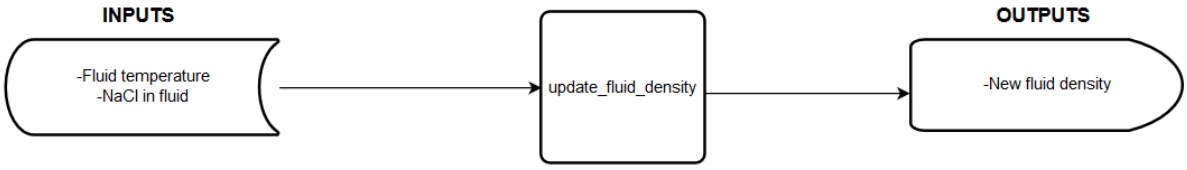

Figure (4.4) Schematic representation of the *update_fluid_density* method in the Interactions class.

4.4.4 Rock Porosity and Fluid pH

The porosity of a rock cell and the fluid's pH are updated through the *update_porosity_ph* method in the Interactions class. This class utilizes the relationships specified in section 3.2.2 to compute new values for the pH and porosity. This method takes as inputs the volume of the incoming fluid to compute the water/rock ratio, the porosity of the current rock cell, the pH of the fluid in associated to the aforementioned rock cell, the neutralization potential of the rock at the specified position and yields a new pH for the fluid, a new neutralization potential and a new porosity for the rock cell in question, as seen in figure 4.5.

Specifically, this method is organized into six sub processes. The first one consists on

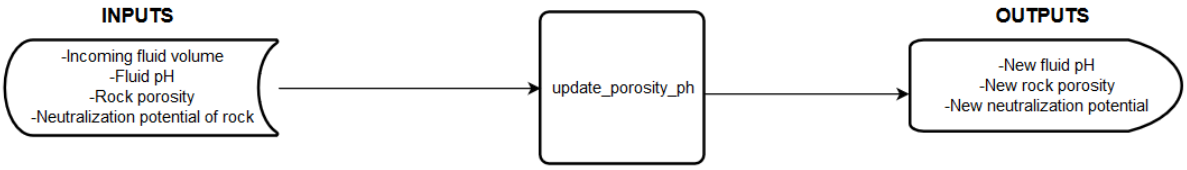

Figure (4.5) Schematic representation of the *update_porosity_ph* method in the Interactions class.

establishing the function 3.19 in order to acquire a resulting fluid pH based on Reed (1997) data. Secondly the water/rock ratio is computed based on the volume of fluid and the densities of both rock and fluid.

Then the inputs used in the processes are obtained. These inputs include the rock porosity, the neutralization potential, simulation decay factors for both pH and porosity, and fluid pH. The next stage consists on obtaining a new fluid pH. Since equation 3.19 is only defined for an initial pH near 1, the linear interpolation described in 3.20 is used.

After computing the new pH, the new porosity is calculated using the linear model of pH variation described in equation 3.24. Finally, all the variables computed in this method are updated.

4.5 Visualizations

Visualizations are made possible through two methods in the Interactions class. One of this methods is the *save_image_status* method which saves the statuses (values) of desired and assigns them color maps which are then drawn using pyplot from matplotlib. These variables are:

- Volume of the fluid
- Pressure of the fluid
- Temperature of the fluid
- Temperature of the rock
- Fluid's pH
- Density of the fluid

These graphic representations of the parameters are then saved into a file.

The other method that creates images of the studied phenomena is the *post_processing* method, which uses the final temperature, depth and pH conditions of the stabilized simulation and creates a map of hydrothermal alterations. These maps are drawn using matplotlib based on the alterations' temperature, pH and depth specified in Chapter 2, Section 2.1.1.

4.6 Running the Simulations and Results of Visualization Methods

In order to run a simulation, certain parameters must be specified to the model. These parameters are:

- Dimensions of the 2D rock grid (number of cells in the vertical and horizontal axes, grid must be square)
- The real life size of each cell (in meters)
- The time interval for each iteration in seconds
- The simulation stabilization time in seconds
- The number of iterations before generating an image result
- The location where the image results ought to be saved
- The range of initial porosity of the rock grid
- The range of initial temperature of the rock grid (based on a geothermal gradient)
- The time (in relation to the simulation) at which the fluid will start and finished to be injected into the rock grid
- The discharge rate at which the fluid will be injected in $[\frac{L}{s}]$
- The initial temperature (in Kelvins) and pH of the fluid
- The NaCl content of the fluid in $[\frac{mole}{1000grams}]$
- The column of the rock grid at which the fluid will be injected

With these parameters the model will be able to run a simulation and yield color maps of the rock grid. These color maps correspond to the rock and fluid temperatures in the rock grid, the fluid's pH at different points of the rock grid, the fluid's density and viscosity and the associated hydrothermal alterations obtained from the interaction between the rock and the fluid as shown in figure 4.6. This figure shows different color maps that represent vertical cross-sections of a porphyry copper deposit.

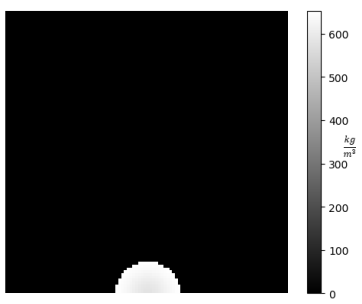

(a)

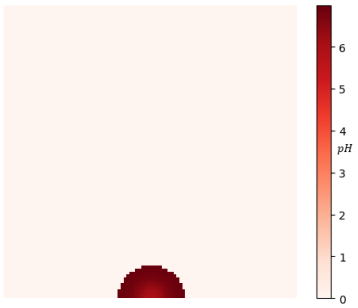

(b)

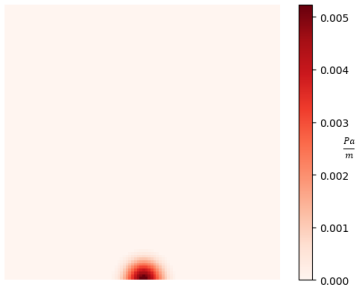

(c)

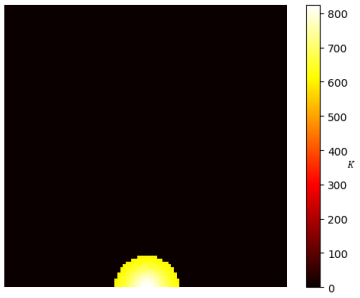

(d)

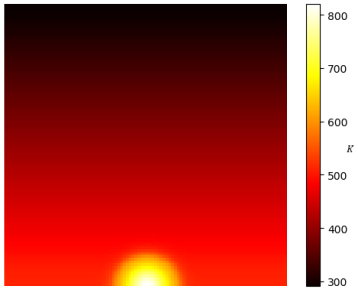

(e)

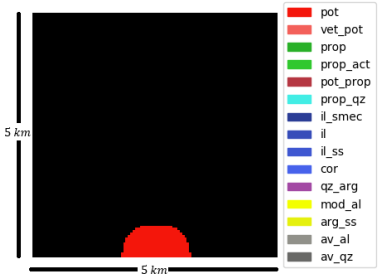

(f)

Figure (4.6) Example color maps for different variables and the alteration zones. These are vertical cross sections of a proposed porphyry copper deposit. (a) Corresponds to the densities of the fluid at different locations in $[\frac{kg}{m^3}]$. (b) Is the pH map of the fluid. (c) Is the pressure map of the fluid distributed inside the rock grid in $[\frac{Pa}{m}]$. (d) Shows the temperature of the fluid (in Kelvins) at different locations within the rock grid. (e) Shows the initial temperature (in Kelvins) of the rock grid. This initial temperature represents a standard geothermal gradient. (f) Shows the resulting hydrothermal alterations of the rock–fluid interaction.

Chapter 5

Results and Discussions

Test runs were concocted in order to analyze the performance of the model under specific circumstances. The results of these test runs are then analyzed together with the overall performance of the model and veracity of its results compared to the known geological models, mainly Sillitoe (2010). Finally, the source of possible flaws or non-realistic results is analyzed so that improvements can be proposed.

5.1 Proposed Tests

The proposed tests are done in order to test if the different fluid-rock interactions specified in the Interactions class are functioning coherently. Therefore, tests for each major method in this class are proposed. The tests are grouped into categories which refer to the interaction being tested. The tests that pertain to a specific method, keep the parameters associated to other methods constant. These categories are:

- Movement and Viscosity Tests
- Thermal Exchange Tests
- Density Variation Tests
- pH and Porosity Variation Tests
- Compound Tests

The compound tests are oriented to test the algorithm in its entirety. That is to say, the overall performance of all the interactions working simultaneously updating all the associated parameters.

5.1.1 Movement Tests

In order to evaluate the correct functioning of the *fluid_ movement* method in the Interactions class the porosity of the rock grid is altered. This is because according to equation 3.5, the movement of the fluid is dependent on permeability, which in turn is dependent on porosity in this model. The following tests are performed:

- Set a plane (line in this case because of 2D model) of higher porosity in the grid
- Set a plane of zero porosity
- Set porosity progressively smaller towards the surface of the grid
- Set the whole grid with zero porosity except for a plane

In the first test the fluid is expected to move following the plane of high porosity because the permeability in that plane will be higher, therefore the discharge per unit area would tend to be higher in those positions.

In the second test the fluid is expected not to be able to flow through the impermeable plane, that is since the permeability is zero, according to equation 3.1, the discharge per unit area will be zero.

In the third test, with a porosity progressively smaller towards the surface of the grid, the fluid is expected to take longer to ascend. This is due to a lower permeability, therefore a lower discharge per unit area.

In the last test, the fluid is expected to only ascend following the permeable plane. Since the rest of the rock grid is impermeable, the fluid will not be able to flow through it.

5.1.2 Thermal Exchange Tests

In order to test the *thermal_ exchange* method the temperature of the fluid is altered. The starting temperature of the fluid is set to room temperature (25°C). The temperature of the fluid is expected to increase due to the higher temperature of the surrounding rock. In this case the rock will be heating the fluid and not the other way around.

5.1.3 Density Variation Tests

In order to test the *update_fluid_ density* method in the Interactions class a test based on the fluid's temperature is proposed. The test consists on keeping the temperature constant during a simulation, acquiring the density of the fluid during that simulation and then comparing it to the density of a second simulation with constant temperature, but this temperature is be lower than the first simulation's. The fluid density of the second simulation is expected to be higher according to equation 3.15 because the temperature dependent term in this equation is inversely proportional to the density.

5.1.4 pH and Porosity Variation Tests

In order to test the *update_porosity_ph* method in the Interactions class the neutralization potential of the rock is set to a large number. Under these conditions the pH of the fluid should remain constant, equal to its initial pH. This is because the neutralization potential works as a counter. When the counter is larger, the rock's capacity to neutralize the fluid is less. Therefore, if the neutralization potential counter is sufficiently large, the rock should not be able to to change the fluid's initial pH.

5.1.5 Compound Tests

In this test the Interactions class is tested in its entirety. Two tests are performed. The first test consists on setting a higher porosity plane in the rock grid. It is expected that the fluid follows this plane, but in addition to that, it is expected that the temperature will also follow this path. The other test consists on injecting multiple fluids in the same position one after the other with different temperature and NaCl content. This is done in order to mirror the change over time of the geothermal system seen in figure 2.6.

5.2 Results of Proposed Tests

It is important to note that the lower or higher porosity planes on the different tests are set to the middle column of the grid. The grids being used in all these tests are 100 by 100 cells, therefore the differential porosity planes are set vertically on the 50th column at the bottom of the grid. Each cell has a dimension equivalent to 50[m]. In all the presented tests, the fluids are injected into the 50th column at the bottom of the grid. It is important to mention that the fluid being injected in all of the tests performed has a speed of $0.001\frac{m}{s}$. This is based on the hydrothermal fluid discharges measured by McMillan (2018) and Fisher et al. (2003). (2003).

Taking into account that the common lifespan of an Andean porphyry copper deposit is around 2.5- to 4-m.y. (Sillitoe & Mortensen, 2010), a coherent time interval for an iteration is proposed. Each iteration represents 10,000 years. The following figures are divided in six sub-figures which exhibit iterations 1, 5, 11, 25, 61, 71. Sub-figure (a) Corresponds to the initial state when time is 0. (b) Corresponds to 50,000 years after the initial state; (c) = 110,000 years; (d) = 250,000 years; (e) = 610,000 years and (f) = 710,000 years. Finally, all of the figures presented in this section correspond to 5 km by 5 km vertical cross-sections of a modeled porphyry copper deposit.

5.2.1 Movement and Viscosity Results

For comparison a standard simulation run is performed. The porosity of the grid in this test is set to be progressively higher towards the surface. Starting with a porosity of 25% at the bottom and a porosity of 30% at the top of the grid. The sequential evolution of the fluid's position is shown in figure 5.1. The porosity is set to be progressively higher towards the top to account for the progressively lower lithostatic pressure and surface erosion.

All the results presented in this section are snapshots of the fluid's presence at the same time intervals. That is to say figure 5.1.(a) is taken at the same simulation time of 5.2.(a) and so on for every other test. This is done in order to establish a valid comparison. In this case, to analize the fluid's presence a map of the fluid's density is shown. The density is not what is being studied in these tests, but it shows the location where the fluid is present, which is what is being analyzed in the movement tests.

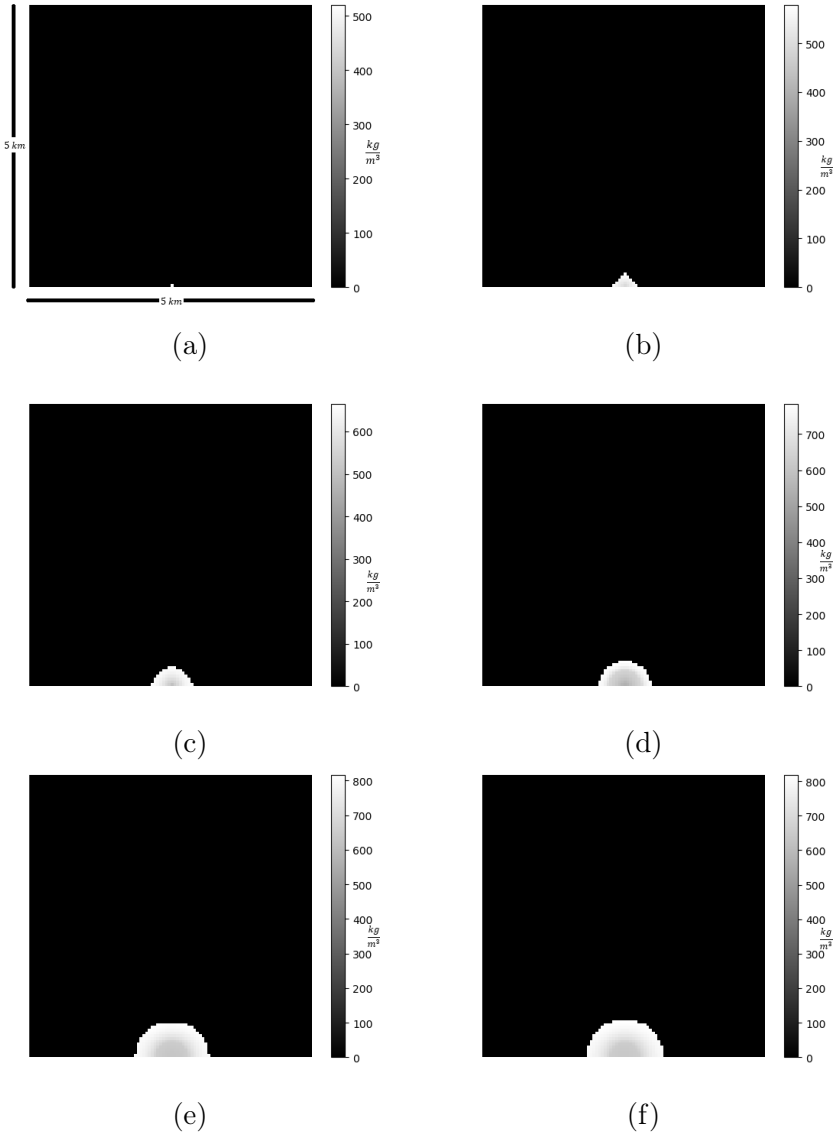

Figure (5.1) The fluid's presence evolution under standard simulation settings. Sub-figures (a)-(f) are in chronological order separated by a fixed time interval.

Plane of Higher Porosity

In order to perform this test, a plane of porosity = 100% is set in the middle of the grid. The fluid's presence evolution when establishing a plane of higher porosity is shown below in figure 5.2. The higher porosity plane is orthogonal to the cross section seen in these figures.

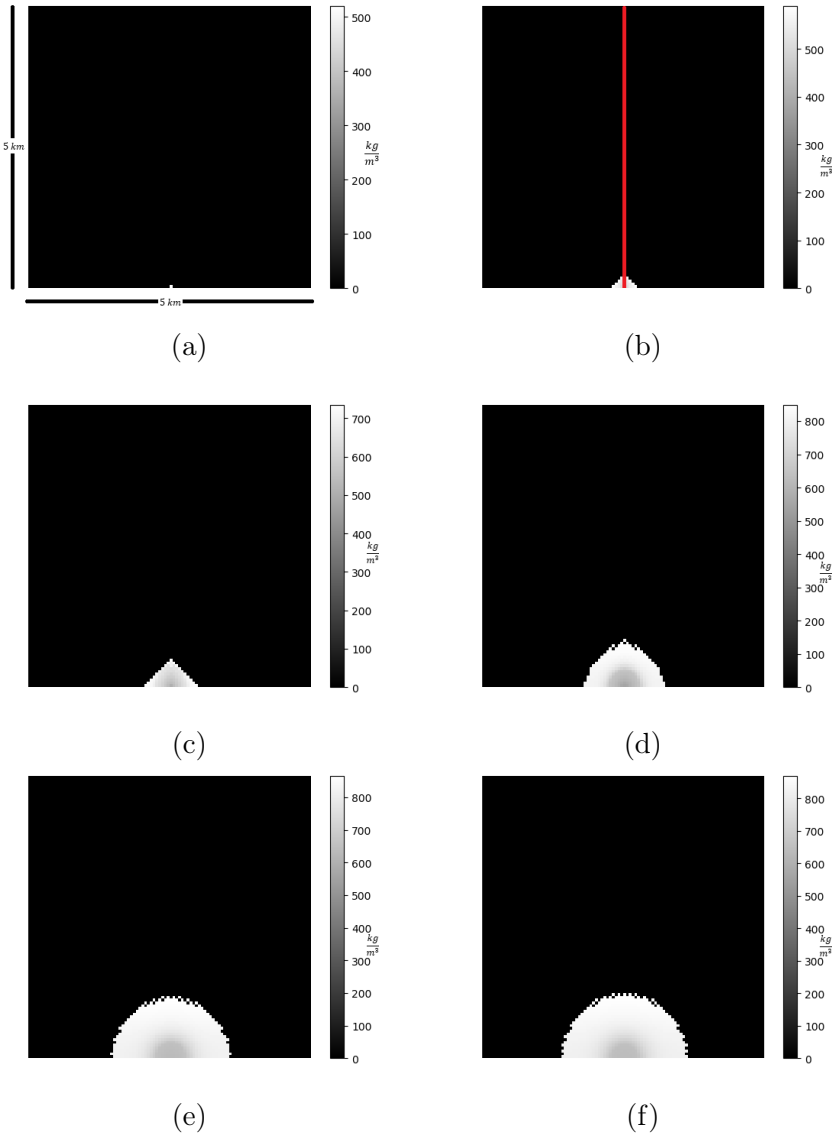

Figure (5.2) The fluid's presence evolution when establishing a plane of higher porosity. Sub-figures (a)-(f) are in chronological order. In sub-figure (b) the higher porosity plane is represented as a red line.

Plane of Zero Porosity

In order to perform this test a plane of porosity = 0.01% is set in the middle of the grid. The fluid's presence evolution when establishing a plane of higher porosity is shown below in figure 5.3. The zero porosity plane is orthogonal to the cross section seen in these figures.

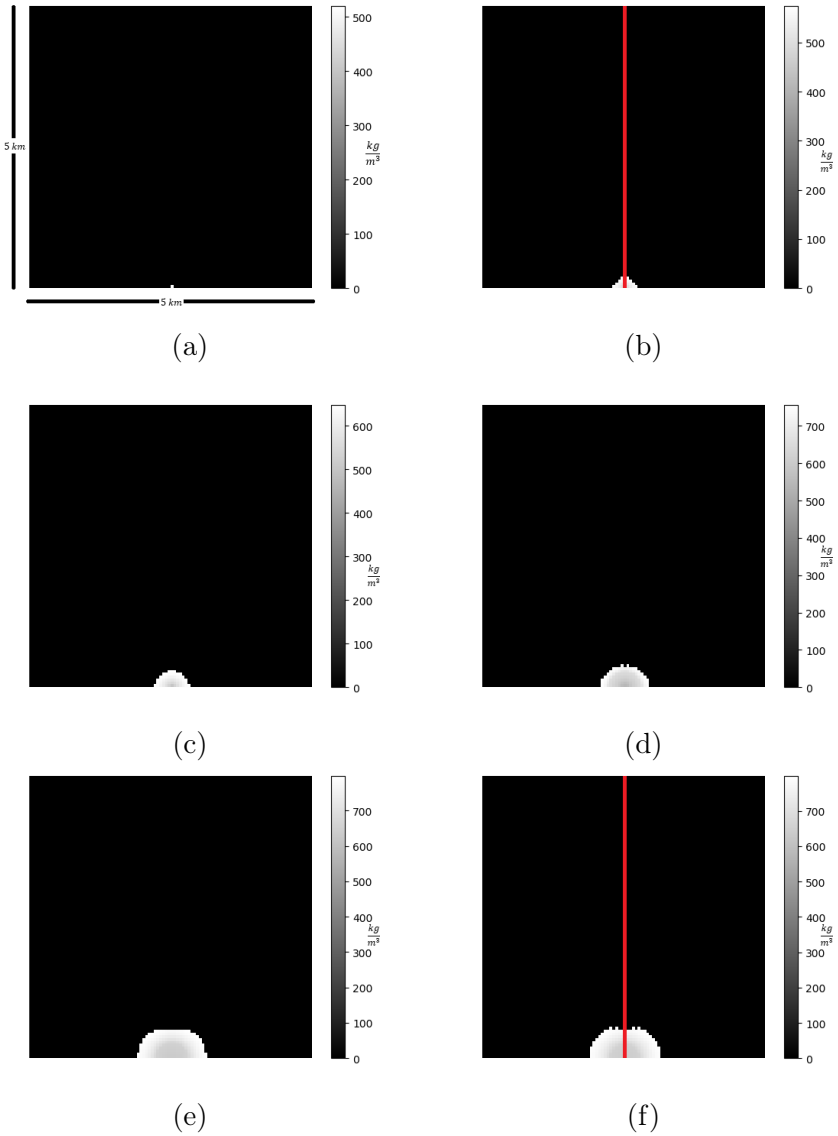

Figure (5.3) The fluid's presence evolution when establishing a plane of lower porosity. Sub-figures (a)-(f) are in chronological order. In sub-figures (b) and (f) the zero porosity plane is represented as a red line.

Porosity Progressively Smaller Towards Surface

In order to perform this test the porosity of the grid is set progressively smaller towards the surface, starting with 30% at the bottom and 25% at the top. The fluid's presence evolution when establishing a progressively lower porosity is shown below in figure 5.4.

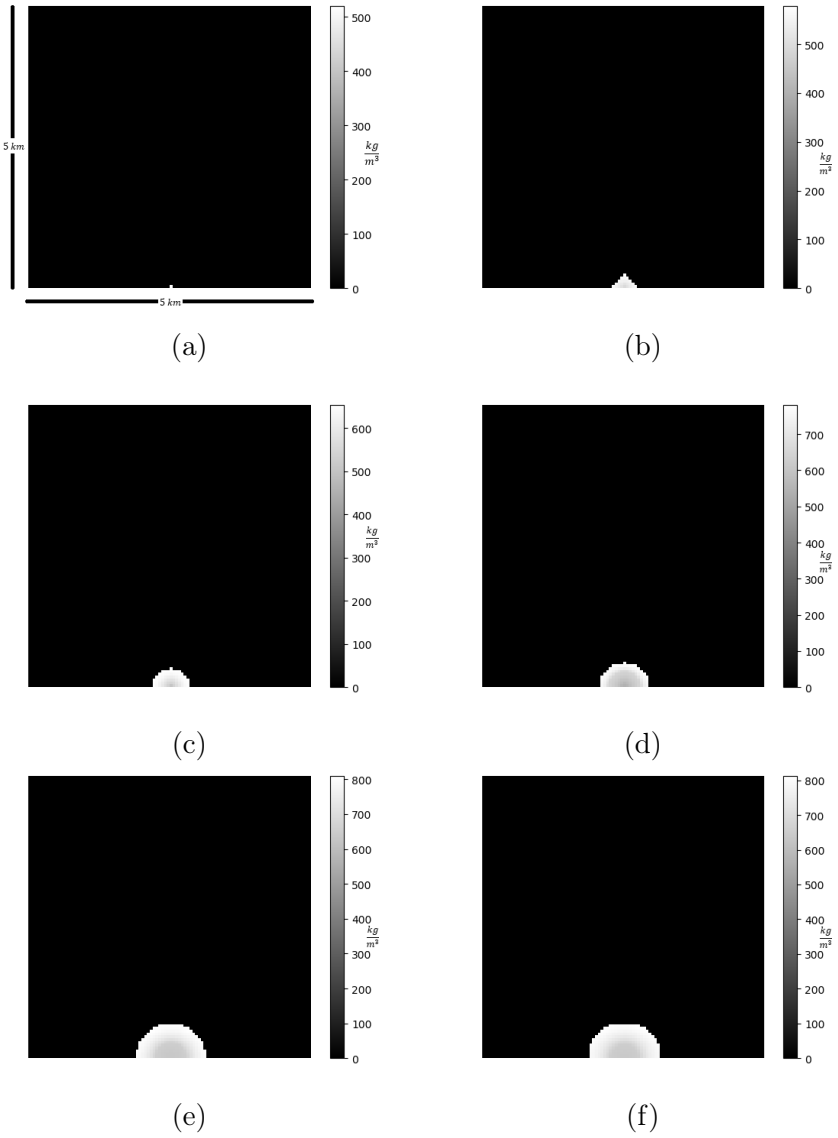

Figure (5.4) The fluid's presence evolution when establishing a progressively lower porosity towards the surface. Sub-figures (a)-(f) are in chronological order.

Porosity Zero except for a Plane

The fluid's presence evolution when establishing zero porosity in the grid except for a plane is shown below in figure 5.5.

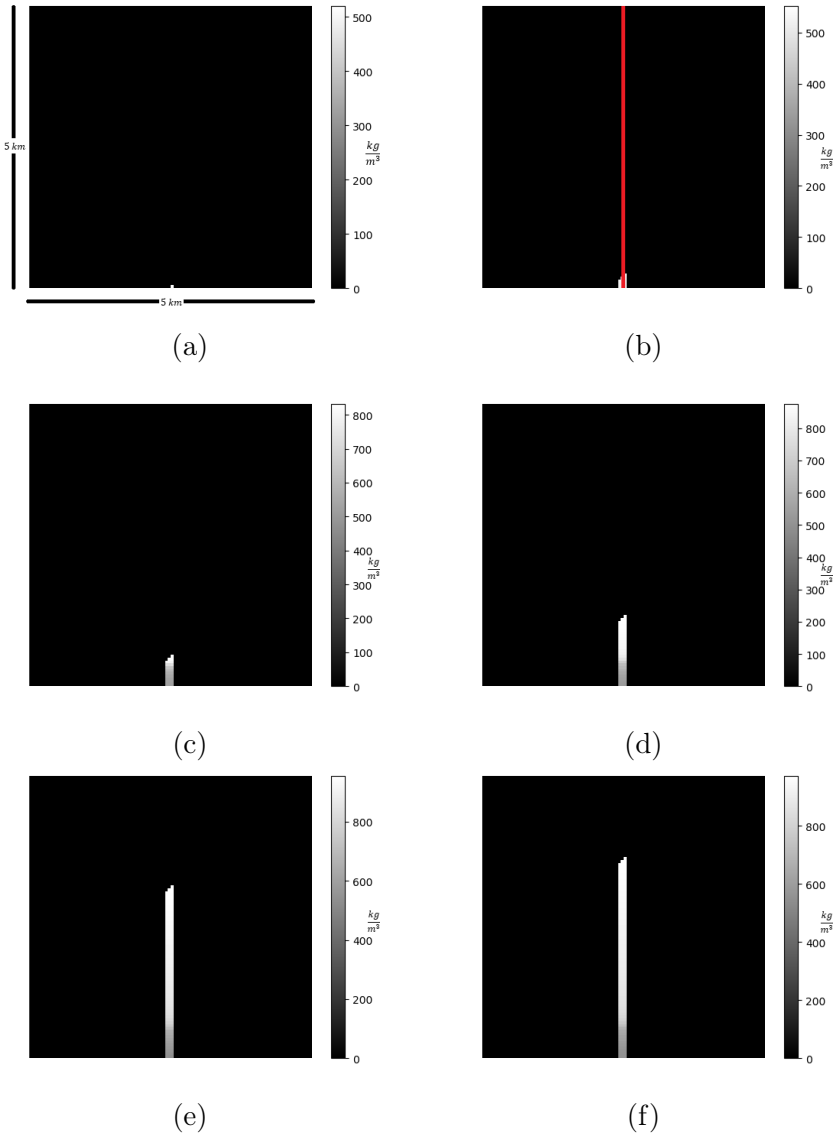

Figure (5.5) The fluid's presence evolution when establishing zero porosity in the grid except for a plane. Sub-figures (a)-(f) are in chronological order. In sub-figure (b) the porosity plane is represented as a red line.

5.2.2 Thermal Exchange Results

For comparison a standard simulation run is performed. The initial temperature is set to 800°C and the temperature ranges of the rock is set to 246.75°C at the bottom and 10°C at the top of the rock grid in order to emulate the geothermal gradient (seen in 4.6.e) (Muñoz & Hamza, 1993). The results for the standard simulation run are shown in figure 5.6. The temperature scale in the figures seen in this sections is in Kelvins.

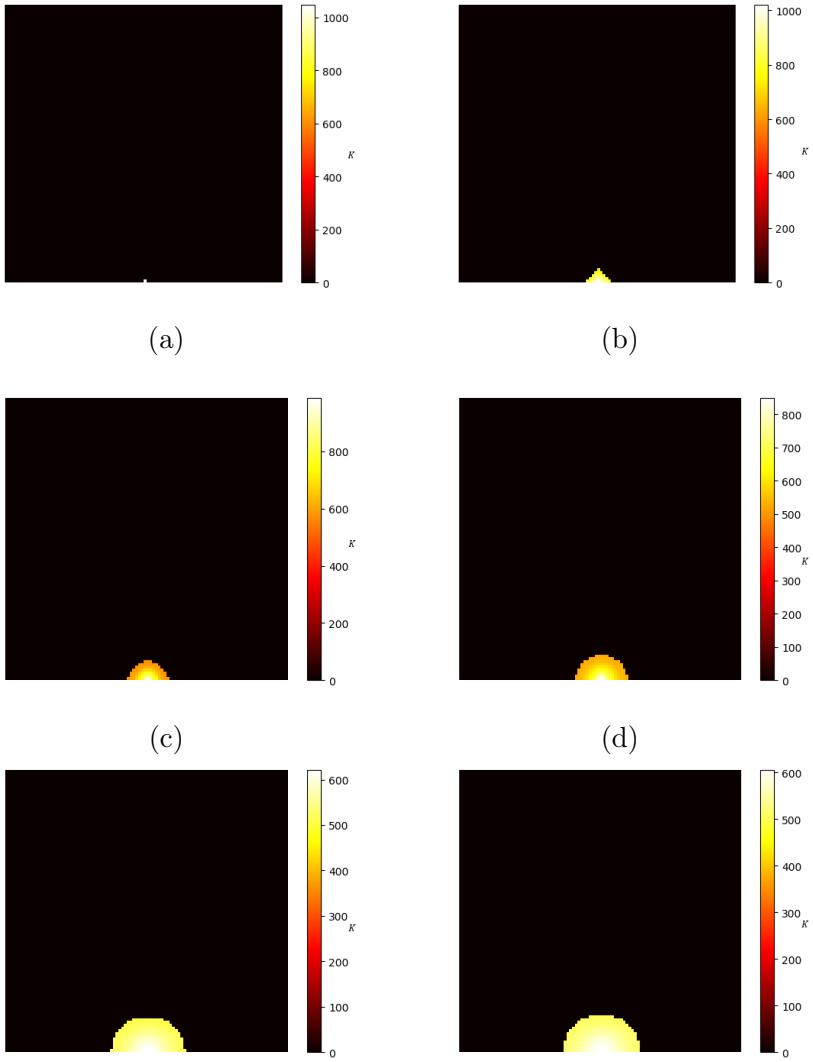

Figure (5.6) The fluid's temperature evolution when being set to an initial temperature of 800 °C. Sub-figures (a)-(f) are in chronological order.

When the fluid is initialized with a temperature of 25°C, the thermal evolution can be seen in figure 5.7. It is important to notice the difference in scale of both figures.

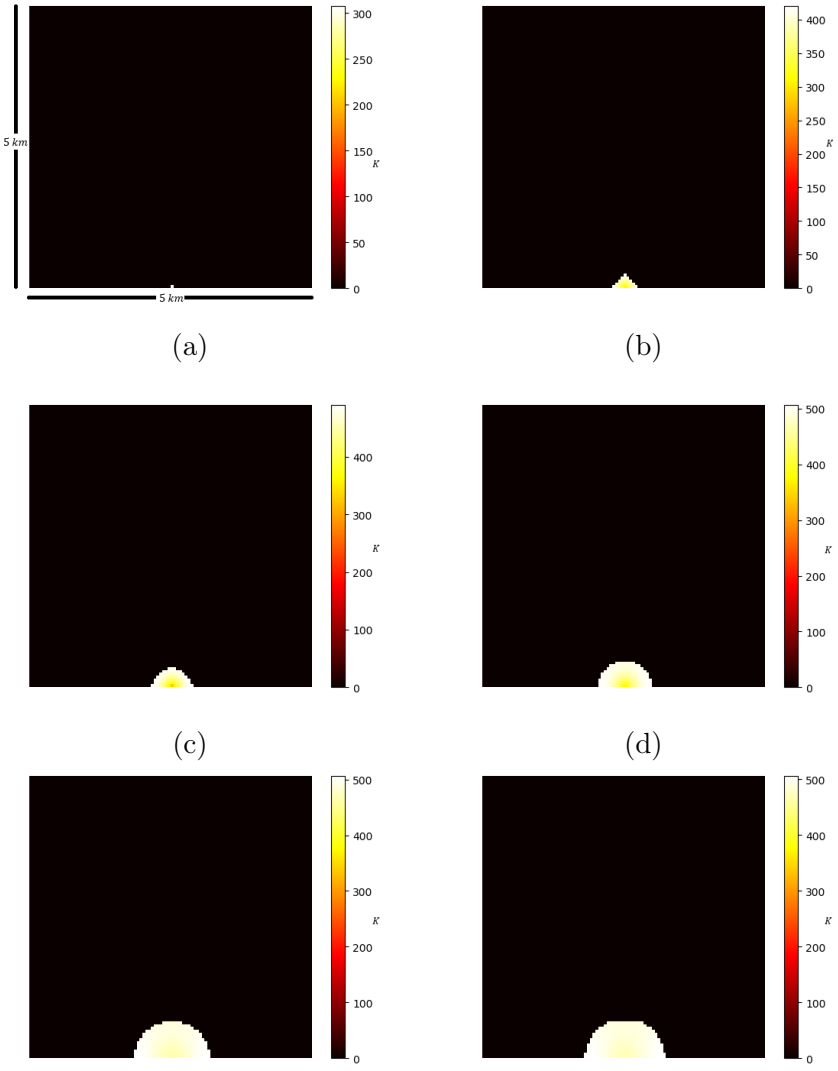

Figure (5.7) The fluid's temperature evolution when being set to an initial temperature of 25 °C. Sub-figures (a)-(f) are in chronological order.

5.2.3 Density Variation Results

In order to test the density interactions, the thermal exchange method is shut off, therefore there is no temperature variation in the fluid. Since the density is temperature dependent (equation 3.15). For comparison a simulation under the previously stated conditions is done with the fluid's temperature at 800°C. The density results for this test run are shown in figure 5.8. The density scale (gray scale) seen in the figures of this section are in $[\frac{kg}{m^3}]$.

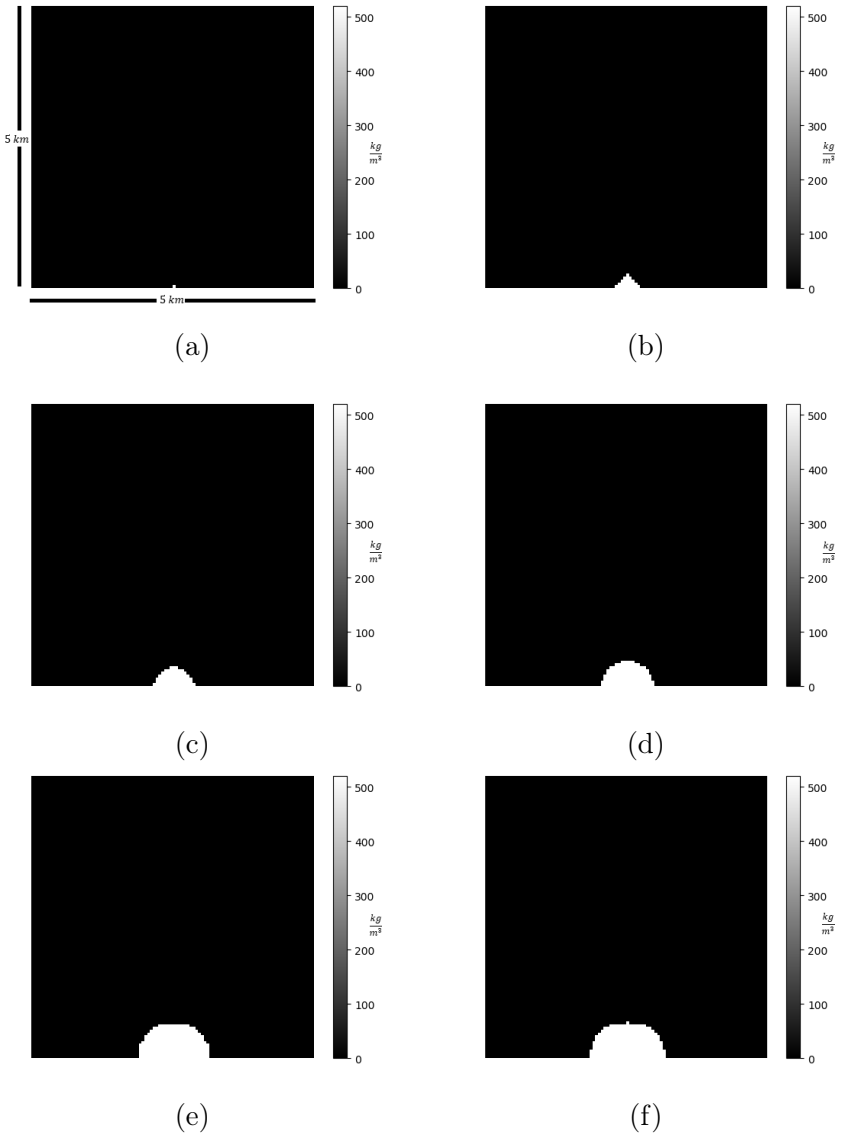

Figure (5.8) The fluid's density without temperature variation, with initial fluid temperature of 800°C. Sub-figures (a)-(f) are in chronological order.

It is possible to observe that the density of the fluid is maintained at around 500 $\frac{kg}{m^3}$,

When the fluid is initialized with a temperature of 25°C, the density evolution can be seen in figure 5.9. It is important to highlight that the temperature of the fluid is set this low only for algorithm testing and not to represent a real-life fluid.

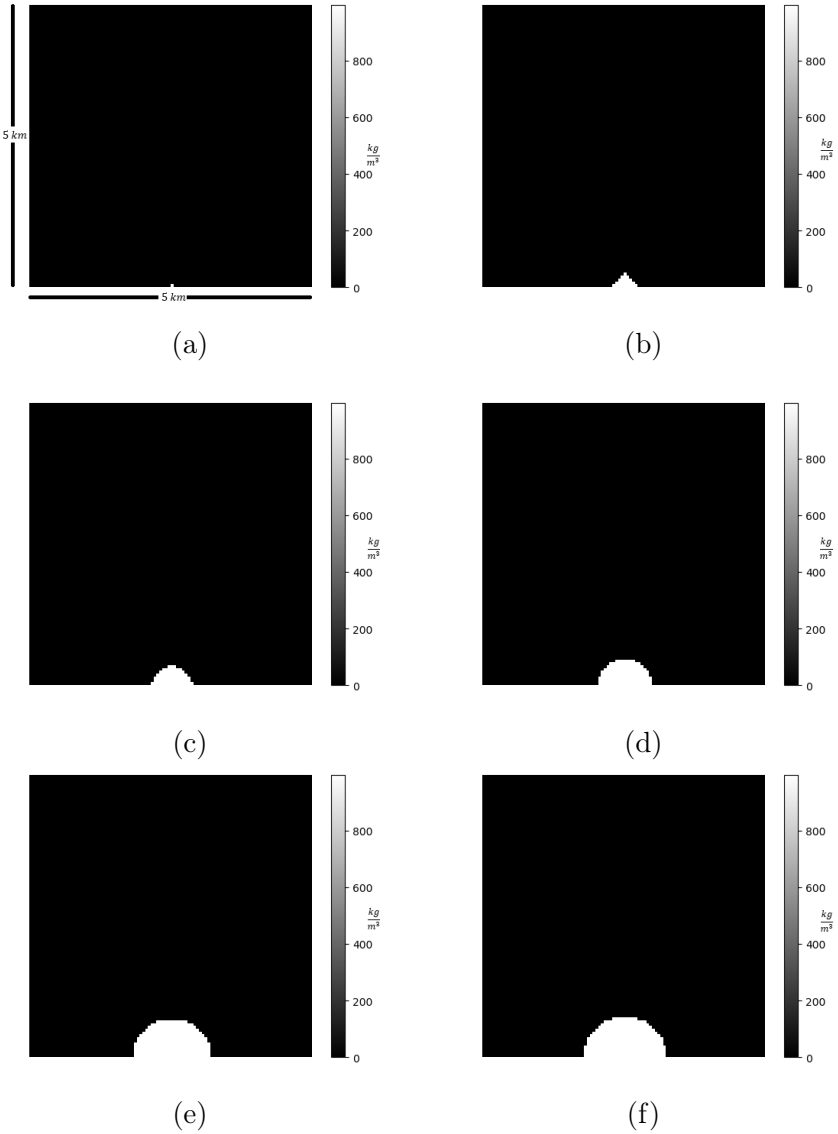

Figure (5.9) The fluid's density without temperature variation, with initial fluid temperature of 25°C. Sub-figures (a)-(f) are in chronological order.

It is possible to observe that the density of the fluid is maintained constant at around 900 $\frac{kg}{m^3}$.

5.2.4 pH and Porosity Variation Results

In order to test the pH variation the aim is to observe if the rock loses the ability to change the pH of the fluid that it interacts with. Based on the fact that over time the buffer series minerals of a rock are lost when in contact with an acid fluid (Reed, 1997), the rock will lose the ability to neutralize a fluid after being exposed to acidic solutions for prolonged periods of time. For comparison purposes, the pH variation of the fluid over time when the neutralization potential counter is initially set to zero is shown in figure 5.10. In these tests the initial fluid's pH is 1. The scale in these figures is in pH values.

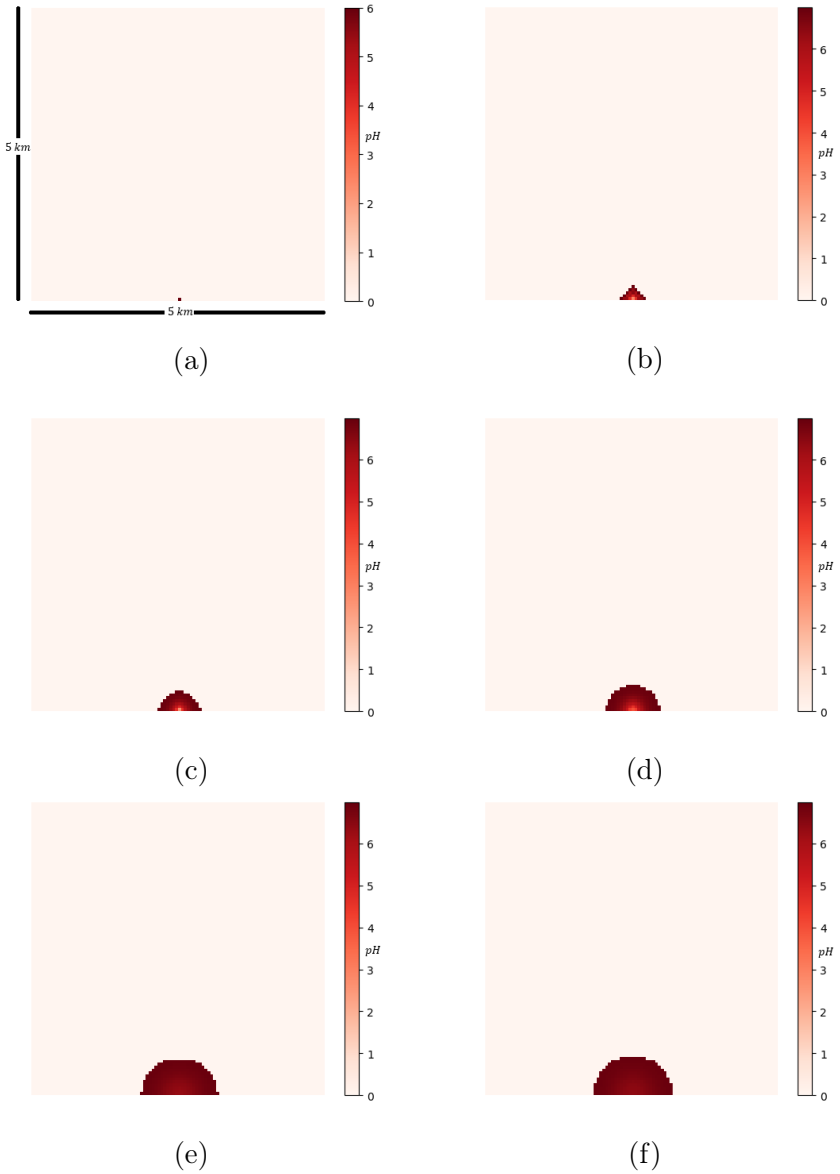

Figure (5.10) The fluid's pH variation while the rock's neutralization potential counter is initially set to zero. Sub-figures (a)-(f) are in chronological order.

It is noticeable that the original pH of one is changed when interacting with the rock for an extended period of time. The resulting pH of the fluid-rock interaction is around six. When the rock's neutralization potential counter is initially set to a large number, in this test 1,000, the result is very different, as seen in figure 5.11.

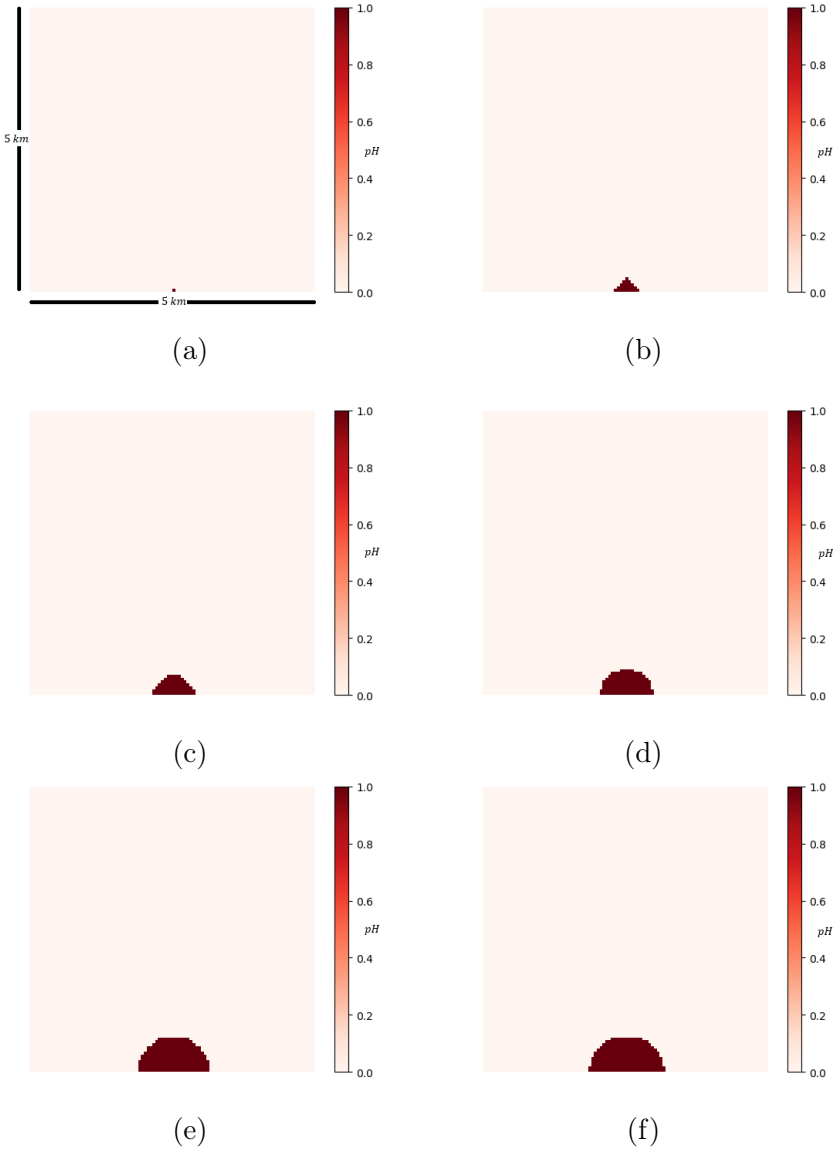

Figure (5.11) The fluid's pH variation while the rock's neutralization potential counter is initially set to zero. Sub-figures (a)-(f) are in chronological order.

The pH scale in figure 5.11 shows that the pH in this figure is constant as time passes by. This constant pH is equal to the initial pH of the fluid, 1. When the rock's neutralization potential is high enough, the rock is not able to change the fluid's pH.

5.2.5 Compound Test Results

In order to test the overall model proposed in this work, a test consisting on setting a higher porosity plane on the rock grid and analyze not just the fluid's presence but the temperature and pH as well. The porosity set on this plane is equal to 100%. All of these parameters can be viewed with an alteration zone map. This is due to the fact that hydrothermal alterations have a defined temperature and pH ranges. The result of a fluid with initial pH of 1 and a temperature of 800°C in a grid with a plane of lower porosity (set to 100%) moving through a rock grid is shown in figure 5.12.

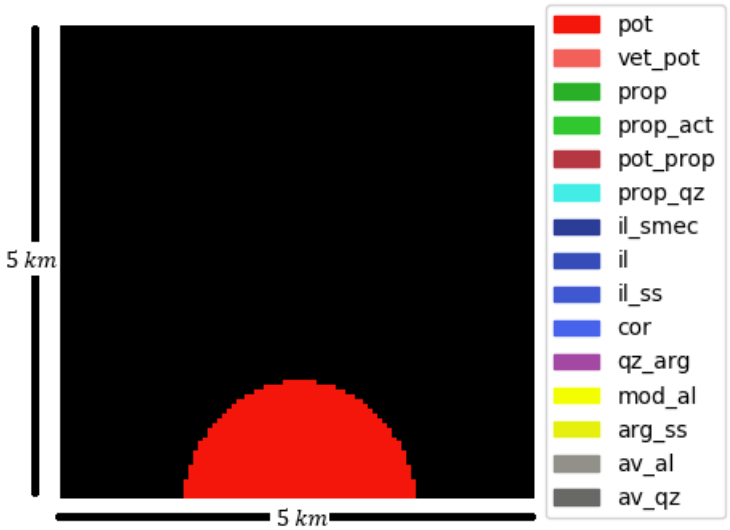

Figure (5.12) Alteration zone map after one fluid injection into the rock grid. pot = Potassic alteration; vet_pot = Potassic alteration with veins; prop = Propylitic alteration; prop_act = propylitic alteration with actinolite; pot_prop = transition between potassic and propylitic alterations; prop_qz = transition between propylitic and sericitic alteration; il_smec = sericitic alteration with illite-smectite assemblages; il = sericitic alteration with predominant illite; il_ss = standard sericitic alteration; cor = sericitc alteration with corundum; qz_arg = transition between sericitic and moderate argillic alteration; mod_al = moderate argillic alterations with alunite; arg_ss = standard moderate argillic alteration; av_al = advanced argillic alteration with alunite; av_qz = advanced argillic alteration with predominantly quartz.

Another test is performed under the same conditions of the previous test. The difference is that in this case seven sequential fluid pulses are introduced. All of the pulses have an initial pH of one, but only the first pulse has an initial temperature of 800°C. The rest of the pulses have an initial temperature of 400°C in order to mirror the temporal evolution of the geothermal system seen in figure 2.6. The results of this test are shown in figure 5.13.

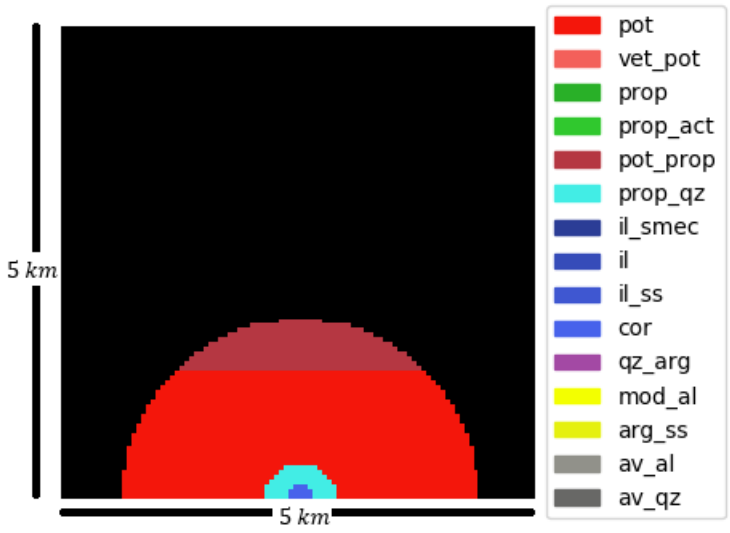

Figure (5.13) Alteration zone map after seven fluid injections into the rock grid. pot = Potassic alteration; vet_pot = Potassic alteration with veins; prop = Propylitic alteration; prop_act = propylitic alteration with actinolite; pot_prop = transition between potassic and propylitic alterations; prop_qz = transition between propylitic and sericitic alteration; il_smec = sericitic alteration with illite-smectite assemblages; il = sericitic alteration with predominant illite; il_ss = standard sericitic alteration; cor = sericitc alteration with corundum; qz_arg = transition between sericitic and moderate argillic alteration; mod_al = moderate argillic alterations with alunite; arg_ss = standard moderate argillic alteration; av_al = advanced argillic alteration with alunite; av_qz = advanced argillic alteration with predominantly quartz.

The prolonged interaction of the rock grid with different fluid pulses causes an alteration zone map with more than one hydrothermal alteration present.

5.3 Analyses

5.3.1 Movement and Viscosity Analysis

Higher Porosity Plane

The reason for setting a plane with a higher porosity than the rest of the grid is in order to simulate a fault plan. Fault planes, and other structures, have a large influence in the upwards flow of hydrothermal fluids (Taillefer et al., 2017; Bouchot et al., 2010). Comparing figure 5.1 (standard porosity) to figure 5.2 (higher porosity plane), one can see that the plane of higher porosity has an effect on the movement of the fluid. The fluid is allowed to flow a greater vertical distance in time intervals (a) through (d) of each respective figure. The most important observation is that at the end of the simulation the fluid is able to reach a much larger distance than without the porosity plane.

Zero porosity plane

This test is performed in order to simulate a zone in which the porosity is lower due to a change of lithology. A more direct connection to the proposed orientation and geometry of the plane is a dyke, which can present lower porosity than the rest of the host rock. Comparing figures 5.1 and 5.3 (plane of zero porosity), it is observable that the columns in which the plane of zero porosity is set (column 50) the fluid does not reach the same distance. The geometry of the fluid's presence at the end of the simulation, sub-figure (f), shows that the central zone had a lesser displacement. Although the plane of zero porosity did not prevent the fluid to move through it, it did retard its movement.

Lower Porosity towards Surface

The reason to model a vertical porosity change is to simulate a change in lithology in host rock. Some lithology presents lower porosity than others. The fluid movement in figure 5.4, associated to a rock grid that gets progressively less porous, does not show much difference to the simulation under standard conditions seen in figure 5.1. The figure shows some delay of the fluid's movement in the vertical axis so that the geometry of the final stage of this figure seems more flattened at the top.

Zero Porosity Grid Except for a plane

In order to simulate the fluid's flow through a highly impermeable rock, the rock grid is set to a null porosity. A plane of high porosity, that could represent a fault plane, is set on this grid. As seen in figure 5.5, the fluid only moves through the plane of high porosity and ignores the rest of the grid. Furthermore, comparing this figure to the one associated with a

high porosity plane in a grid of lower porosity but not equal to zero shown in figure 5.2, one can observe that the fluid was able to reach much farther in the vertical axis. This is due to the fact that when the rest of the grid is set to zero porosity, the fluid tends to move in only one direction (upwards) and not to the sides. The fluid is transported only vertically ignoring the sideways movement. This behavior could be compared to how a vein is obtained in a geothermal system.

5.3.2 Thermal Exchange Analysis

The thermal exchange interactions were tested to observe if the fluid was able to gain temperature when being exposed to a hotter environment. When injecting a high temperature fluid (figure 5.6), the temperature of the fluid progressively decays as time passes by. This differs to the results obtained when injecting a room temperature fluid to a rock grid with a geothermal gradient (figure 5.7). The fluid starts with a low temperature and progressively heats up when interacting with the rock. This shows that the model can account for a fluid gaining temperature when being exposed to a geothermal gradient.

5.3.3 Density Variation Analysis

In order to test if the density responded as expected, the thermal exchange interaction was disabled for this test. When injecting a high temperature fluid (800°C) into the grid the temperature (figure5.8) is seen to maintain a density of around 500 $[\frac{kg}{m^3}]$. When the injected fluid has a temperature of 25°C, the density of the fluid is maintained at around 900 $[\frac{kg}{m^3}]$ which is coherent to the density of water under standard conditions. The density of the fluid efficiently responds to different temperatures.

5.3.4 pH and Porosity Variation Analysis

Considering the rock's ability to neutralize an acidic fluid, figure 5.10 shows the change over time of pH of an initially acidic solution (pH = 1). After interacting with the rock the acidic fluid reaches a pH of around 7. When the neutralization potential of the rock is taken away, one can observe that the initial pH of the fluid is maintained, as seen in figure 5.11. This test is done in order to verify that the model responds coherently to a rock being 'worn down' by prolonged exposure to acid fluids.

5.3.5 Compound Analysis

When setting a higher porosity plane to an already porous grid, the fluid is not only able to move more efficiently, but it can also interact with a greater portion of the host rock. In figure 5.12 one can observe that the overall thermal, pH, and movement interactions produce

a potassic alteration in the host rock. This result is based on the temperature, pH and position in the grid of the fluid. This result shows a correlation with the models proposed by Sillitoe (2010) and Lowell & Guilbert (1970).

When injecting various sequential fluid pulses in order to simulate the fluid's temporal evolution seen in figure 2.6, the model's response is mildly different to the previous test. As shown in figure 5.13, the sequential injections of fluid pulses generates more than one hydrothermal alteration. In this case, a nucleus of sericitic alteration with corundum as an accessory is generated surrounded by a transition between propylitic and sericitic alterations. The bulk of the generated alteration corresponds to a potassic assemblage followed by a transition between potassic and propylitic alterations. This result does not match the described zoning architecture seen in Sillitoe (2010) and Lowell & Guilbert (1970). These authors' models propose that the nucleus should be a potassic core surrounded by sericitic and propylitic alterations. This difference can be due to the fact that all the fluids are injected into the same column. Later stage fluids have lower temperatures and the rock cells they interact with have lost their ability to neutralize their pH. Therefore a more acid fluid with a lower temperature yields propylitic and sericitic alterations. The fact that the grid does not become structurally deformed over time can also be a reason why the zoning does not match the one described in literature. A rock massif can be faulted as time goes by allowing fluids to move through the fault plane into shallower depths. This grid variation is not accounted for in these simulations.

5.4 General Discussions

When introducing lower or higher porosity planes into a porous rock grid, the fluid is not canalized or driven away from these planes as effectively as one may predict. This is due to how the permeability is computed in the *fluid_movement* method in the Interactions class. This method takes a harmonic mean of the permeability between the rock cell in question and its neighbors. Therefore, the lower or higher porosity planes are averaged out by the neighbor cells of lower or higher porosity. This results in the fluid's canalization to not be as abrupt as it is expected to.

Setting the whole grid's porosity to zero except for a plane of high porosity yields a more abrupt fluid canalization. Since averaging a high porosity value with a null one will still yield a positive porosity for the plane, but not for the rest of the grid. When modeling a fault it is perhaps more efficient to set the whole grid's porosity to zero and model the plane differently. In this fashion a stationary domain can be established in which the fluid moves more efficiently.

As seen in figure 5.14, the resulting hydrothermal alterations obtained from the simulations are not exactly coherent with what is seen in literature. This is in part because many of the thermal parameters (specific heat, heat conductivity, heat transfer coefficient and thermal diffusivity) are assumed to be constants. In reality, these parameters vary according to temperature, pressure and state of matter. Another source of error is the fact that the fluid is considered to always be in the liquid state and not split into two (gas and fluid) or

even change into another state such as the supercritical state. Furthermore, the simulations have a time constraint in which the user has to set for how long the fluid is injected and how long after that the fluid is allowed to interact with the rock. When using exponential decays for pH and porosity for example, decay factors are also set by the user given the fact that experimental procedures were not performed in order to set an empirical value. These decay factors were tuned to yield coherent outputs, but the lack of experimental procedures, largely affects the accuracy and precision of the model. Finally some interactions, such as porosity and pH variation, are based on experimental results that were done under specific temperature and pressure conditions. These experiments do not account for porosity loss due to mineralization, therefore porosity is always gained which does not represent the natural phenomena to a full extent. Extrapolating this data to be used outside those temperature and pressure ranges could result in a source of error when computing interactions at these new conditions.

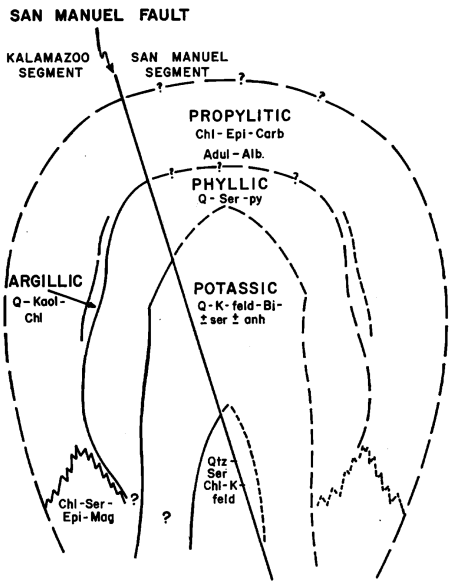

(a)

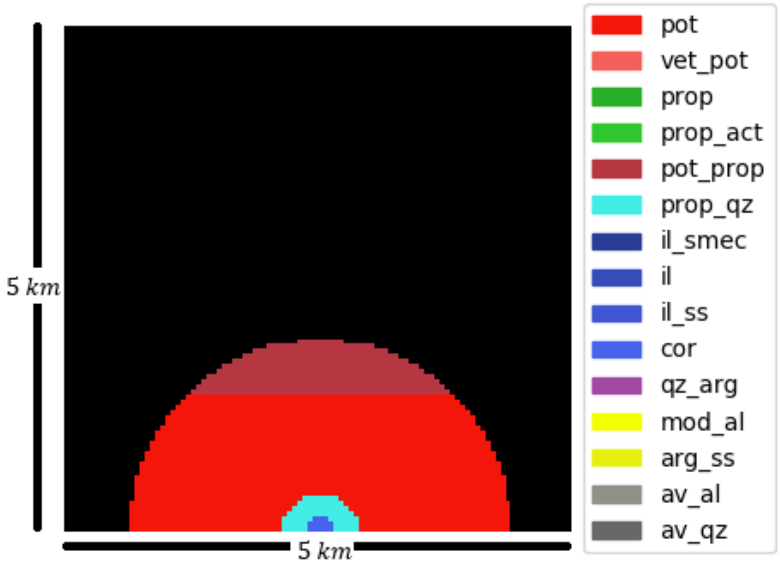

(b)

Figure (5.14) Comparison between traditional porphyry copper model (a) and obtained results (b). Sub-figure (a) is adapted from (Lowell & Guilbert, 1970).

.

Chapter 6

Conclusions and Proposed Research

Porphyry copper deposits are currently the the largest source of copper ore in the world. Although widely explored, there are not many attempts to model their architecture and distribution using computational models. This research aimed to establish a preliminary tool to model the spatial distribution of alteration zones of these types of deposits through discrete computer based algorithms. Comparing the outcome simulations of this model requires a qualitative validation to the simulated parameters as well as provide a tool to produce data to validate models found in literature.

The computer model is generated by basing it the research on widely accepted porphyry copper models in addition to empirical research and existing physical relationships. This model is able to account for a fluid's movement through a porous host rock, the temperature exchange between these two objects, the fluid's pH variation through time and other parameter variation such as the fluid's density and viscosity. Using the fluid's pH, position and temperature, a map of hydrothermal alteration zones is obtained. This alteration zone map is compared to traditional porphyry copper models in order to validate the model.

Validation tests for the different modeled interactions were performed with results that met, to a degree, what was expected. The comparison between the output alteration zone map and the schematic representations of porphyry copper models does not result in an exact match. This difference can be attributed to the simplification of how some parameters are acquired and data interpolation due to lack of experimental results.

In order to produce better results the acquisition of experimental data for the following parameters is proposed. The pH variation of a fluid when it interacts with a rock over a large range of temperature. In this study the pH variation function is based on the experimental results of Reed (1997), which was done only for the acid alteration of andesite at 300°C. It is highly probable that the behavior of this pH variation is different at different temperatures and even pressures. Replicating the simulation with different lithologies is also recommended since in this model only andesite was considered. The pH and porosity variation could be studied for other types of igneous rocks as well as sedimentary rocks, especially limestone. Limestone presents an interesting topic because of a possible skarn assemblage. Furthermore, it is advised to account for the temperature and pressure dependency of thermal parameters

such as specific heat, heat conductivity, heat transfer coefficient and thermal diffusivity. In this model these parameters are considered to be constant but in reality they vary under different conditions. Each of these variation requires arduous research in their own right. The more in depth study of these parameters were not considered in this research due to the fact that this level of specification is without the necessary time constraints as well as the lack of experimental studies.

Finally, this computational model shows a promising initiative to replicate field and experimental based models with discrete simulations. Although the results do not exactly match the widely accepted models for porphyry copper, they bare an undeniable resemblance to them.

Bibliography

Alt-Epping, P., & Smith, L. (2001). Computing geochemical mass transfer and water/rock ratios in submarine hydrothermal systems: implications for estimating the vigour of convection. *Geofluids*, *1*(3), 163-181. Retrieved from https://onlinelibrary.wiley.com/doi/abs/10.1046/j.1468-8123.2001.00014.x doi: 10.1046/j.1468-8123.2001.00014.x

Amilibia, A., Sàbat, F., McClay, K., Muñoz, J., Roca, E., & Chong, G. (2008). The role of inherited tectono-sedimentary architecture in the development of the central andean mountain belt: Insights from the cordillera de domeyko. *Journal of Structural Geology*, *30*(12), 1520–1539.

Apel, M. (2006). From 3d geomodelling systems towards 3d geoscience information systems: Data model, query functionality, and data management. *Computers & Geosciences*, *32*(2), 222 - 229. Retrieved from http://www.sciencedirect.com/science/article/pii/S0098300405001524 doi: https://doi.org/10.1016/j.cageo.2005.06.016

Arai, K., Basuki, A., & Harsono, T. (2012). Hot mudflow prediction area model and simulation based on cellular automata for lusi mud plume at sidoarjo in east java. *Journal of Computational Science*, *3*(3), 150 - 158. Retrieved from http://www.sciencedirect.com/science/article/pii/S1877750311000901 (Scientific Computation Methods and Applications) doi: https://doi.org/10.1016/j.jocs.2011.10.004

Asagba, P. O., & Ogheneovo, E. E. (2008). A comparative analysis of structured and object-oriented programming methods. *Journal of Applied Sciences and Environmental Management*, *12*(4).

Bear, J. (2013). *Dynamics of fluids in porous media*. Courier Corporation.

Besson, U. (2012, Aug 01). The history of the cooling law: When the search for simplicity can be an obstacle. *Science & Education*, *21*(8), 1085–1110. Retrieved from https://doi.org/10.1007/s11191-010-9324-1 doi: 10.1007/s11191-010-9324-1

Bouchot, V., Traineau, H., Guillou-Frottier, L., Thinon, I., Baltassat, J.-M., Fabriol, H., ... Lasne, E. (2010, April). Assessment of the Bouillante Geothermal Field (Guadeloupe, French West Indies): Toward a Conceptual Model of the High Temperature Geothermal System. In I. G. Association (Ed.), *World Geothermal Congress 2010* (p. 8 p.). Bali, Indonesia. Retrieved from https://hal-brgm.archives-ouvertes.fr/hal-00493695

Chailloux, E., Manoury, P., & Pagano, B. (2007). Developing applications with objective caml. 2007. *Developement d'applications avec Objective Caml*.

Corbett, G. J., & Leach, T. M. (1998). *Southwest Pacific Rim Gold-Copper Systems: Structure, Alteration, and Mineralization*. Society of Economic Geologists. Retrieved from https://dx.doi.org/10.5382/SP.06 doi: 10.5382/SP.06

Cracknell, M. (2014). *Machine learning for geological mapping: Algorithms and applications*

(Unpublished doctoral dissertation). University of Tasmania.

de Oliveira Barros, K., Ribeiro, C. A. A. S., Marcatti, G. E., Lorenzon, A. S., de Castro, N. L. M., Domingues, G. F., ... dos Santos, A. R. (2018). Markov chains and cellular automata to predict environments subject to desertification. *Journal of Environmental Management*, *225*, 160 - 167. Retrieved from http://www.sciencedirect.com/science/article/pii/S0301479718308223 doi: https://doi.org/10.1016/j.jenvman.2018.07.064

Domeyko, I. (1876). Jeolojia minera. ensayo sobre los depósitos metalíferos de chile, con relacion a su jeolojía i configuracion esterior. *Anales de la Universidad de Chile*, ág. 441–582. Retrieved from https://revistas.uchile.cl/index.php/ANUC/article/view/19339 doi: 10.5354/0717-8883.2012.19339

Drummond, S. (1981). *Boiling and mixing of hydrothermal fluids: Chemical effects on mineral precipitation.* (Memoria para optar al grado de Licenciada en Ciencias de la Ingeniería y al título de Ingeniera Civil en Computación e Informática). The Pennsylvania State University, Antofagasta.

Emmons, W. H. (1927). Relations of the disseminated copper ores in porphyry to igneous intrusives. *Mining and Metallurgy*(1638-I), 797–815.

Eppelbaum, L., Kutasov, I., & Pilchin, A. (2014). Thermal properties of rocks and density of fluids. In *Applied geothermics* (pp. 99–149). Berlin, Heidelberg: Springer Berlin Heidelberg. Retrieved from https://doi.org/10.1007/978-3-642-34023-9_2 doi: 10.1007/978-3-642-34023-9_2

Fisher, A., Davis, E., Hutnak, M., Spiess, V., Zühlsdorff, L., Cherkaoui, A., ... others (2003). Hydrothermal recharge and discharge across 50 km guided by seamounts on a young ridge flank. *Nature*, *421*(6923), 618.

Fitts, C. R. (2013). 2 - physical properties. In C. R. Fitts (Ed.), *Groundwater science (second edition)* (Second Edition ed., p. 23 - 45). Boston: Academic Press. Retrieved from http://www.sciencedirect.com/science/article/pii/B9780123847058000029 doi: https://doi.org/10.1016/B978-0-12-384705-8.00002-9

Fowler, S. J., Kosakowski, G., Driesner, T., Kulik, D. A., Wagner, T., Wilhelm, S., & Masset, O. (2016, Mar 01). Numerical simulation of reactive fluid flow on unstructured meshes. *Transport in Porous Media*, *112*(1), 283–312. Retrieved from https://doi.org/10.1007/s11242-016-0645-7 doi: 10.1007/s11242-016-0645-7

García, J., Pérez, O., Fdez-Polanco, F., & Cocero, M. (2003). Supercritical water as reaction media. physical properties at supercritical conditions an overview. In *International seminar on aerogels.*

General python faq. (n.d.). Python Software Foundation. Retrieved from https://docs.python.org/3/faq/general.html#what-is-python

Gerakakis, I., Gavriilidis, P., Dourvas, N. I., Georgoudas, I. G., Trunfio, G. A., & Sirakoulis, G. C. (2018). Accelerating fuzzy cellular automata for modeling crowd dynamics. *Journal of Computational Science*. Retrieved from http://www.sciencedirect.com/science/article/pii/S1877750318304022 doi: https://doi.org/10.1016/j.jocs.2018.10.007

Granek, J. (2016). *Application of machine learning algorithms to mineral prospectivity mapping* (Unpublished doctoral dissertation). University of British Columbia.

Haas, J. L. (1971, 10). The effect of salinity on the maximum thermal gradient of a hydrothermal system at hydrostatic pressure. *Economic Geology*, *66*(6), 940-946. Retrieved from

https://doi.org/10.2113/gsecongeo.66.6.940 doi: 10.2113/gsecongeo.66.6.940

Hall, R. W. (1986). Discrete models/continuous models. *Omega*, *14*(3), 213 - 220. Retrieved from http://www.sciencedirect.com/science/article/pii/030504838690040X doi: https://doi.org/10.1016/0305-0483(86)90040-X

Hemley, J., Meyer, C., Hodgson, C., & Thatcher, A. (1967). Sulfide solubilities in alteration-controlled systems. *Science*, *158*(3808), 1580–1582.

Hronsky, J. (2015). The future of mineral exploration–and what it means for geophysics. In *Aseg extended abstracts 2015: 24th international geophysical conference and exhibition* (pp. 1–1).

Klein, D. P., & Johnson, G. R. (1983). *Density, porosity, and magnetic properties of rock specimens from southwestern arizona* (Tech. Rep.). US Geological Survey,.

Korson, L., Drost-Hansen, W., & Millero, F. J. (1969). Viscosity of water at various temperatures. *The Journal of Physical Chemistry*, *73*(1), 34-39. doi: 10.1021/j100721a006

Kumar, S., & Srivastava, P. (2014). Hydrothermal fluids of magmatic origin. In *Modelling of magmatic and allied processes* (pp. 181–208). Springer.

Lindgren, W. (1933). *Mineral deposits* (Fourth Edition ed.). New York and London: McGraw-Hill Book Company, Inc.

Lowell, J. D. (1968). Geology of the kalamazoo orebody, san manuel district, arizona. *Economic Geology*, *63*(6), 645–654.

Lowell, J. D., & Guilbert, J. M. (1970). Lateral and vertical alteration-mineralization zoning in porphyry ore deposits. *Economic Geology*, *65*(4), 373–408.

Matyka, M., Khalili, A., & Koza, Z. (2008, Aug). Tortuosity-porosity relation in porous media flow. *Phys. Rev. E*, *78*, 026306. Retrieved from https://link.aps.org/doi/10.1103/PhysRevE.78.026306 doi: 10.1103/PhysRevE.78.026306

McMillan, N., Larson, P., Fairley, J., Mulvaney-Norris, J., & Lindsey, C. (2018). Direct measurement of advective heat flux from several yellowstone hot springs, wyoming, usa. *Geosphere*, *14*(4), 1860–1874.

Meyer, C. (1957). Hydrothermal alteration in some granodiorites. *Clays and Clay Minerals*, *6*, 89–100.

Meyer, C. (1965). An early potassic type of wall-rock alteration at butte, montana. *American Mineralogist*, *50*(10), 1717–1722.

Meyer, C. (1967). Wall rock alteration. *Geochemistry of hydrothermal ore deposits*, 166–235.

Miranda, O. (2017). *Optimización de algortimos para un simulador de flujo granular* (Memoria para optar al grado de Licenciada en Ciencias de la Ingeniería y al título de Ingeniera Civil en Computación e Informática). Universidad Católica del Norte, Antofagasta.

Muñoz, M., & Hamza, V. (1993, Sep 01). Heat flow and temperature gradients in chile. *Studia Geophysica et Geodaetica*, *37*(3), 315–348. Retrieved from https://doi.org/10.1007/BF01624604 doi: 10.1007/BF01624604

Norton, D. L. (1984). Theory of hydrothermal systems. *Annual Review of Earth and Planetary Sciences*, *12*(1), 155–177.

Padovani, D., Neto, J. J., & Cereda, P. R. M. (2018). Modeling pedestrian dynamics with adaptive cellular automata. *Procedia Computer Science*, *130*, 1120 - 1127. Retrieved from http://www.sciencedirect.com/science/article/pii/S1877050918305313 (The 9th International Conference on Ambient Systems, Networks and Technologies (ANT 2018) / The 8th International Conference on Sustainable Energy Information Technology (SEIT-2018) / Affiliated Workshops) doi: https://doi.org/10.1016/j.procs.2018.04.165

Perlman, H. (2018). *Heat capacity of water.* U.S. Geological Survey. Retrieved from http://water.usgs.gov/edu/heat-capacity.html

Potter, R. W., & Brown, D. L. (1975). *The volumetric properties of aqueous sodium chloride solutions from 0 degrees to 500 degrees c at pressures up to 2000 bars based on a regression of the available literature data* (Tech. Rep.). US Geological Survey,.

Producción cobre de mina mundial y chile. (2018). COCHILCO. Retrieved from https://www.cochilco.cl/Paginas/Estadisticas/BasesdeDatos/Producción-Minera.aspx (Accessed: 2019-01-09)

Reed, M. H. (1997). Hydrothermal alteration and its relationship to ore fluid composition. *Geochemistry of hydrothermal ore deposits*, *1*, 303–365.

Robertson, E. C. (1988). *Thermal properties of rocks* (Tech. Rep.). US Geological Survey,.

Rocca, H. (2005). *Sistemas, modelos y simulación.* Retrieved from <http://materias.fi.uba.ar/7526/docs/teoria.pdf> (Universidad de Buenos Aires)

Roy, S. (2019). A study on delay-sensitive cellular automata. *Physica A: Statistical Mechanics and its Applications*, *515*, 600 - 616. Retrieved from http://www.sciencedirect.com/science/article/pii/S0378437118313359 doi: https://doi.org/10.1016/j.physa.2018.09.195

Scarfe, C. M., & Cronin, D. J. (1986). Viscosity-temperature relationships of melts at 1 atm in the system diopside-albite. *American Mineralogist*, *71*(5-6), 767–771.

SERNAGEOMIN. (2018, apr). *Anuario de la minería de chile 2017* (Tech. Rep.). Santiago, Chile: Servicio Nacional de Geología y Minería.

Sharma, P. (2002). Environmental and engineering geophysics cambridge university press cambridge. *United Kingdom*.

Sillitoe. (1972). A plate tectonic model for the origin of porphyry copper deposits. *Economic geology*, *67*(2), 184–197.

Sillitoe. (1973). The tops and bottoms of porphyry copper deposits. *Economic Geology*, *68*(6), 799–815.

Sillitoe. (2000). Styles of high-sulphidation gold, silver and copper mineralisation in porphyry and epithermal environments. In *Proceedings of the australasian institute of mining and metallurgy* (Vol. 305, pp. 19–34).

Sillitoe. (2010). Porphyry copper systems. *Economic geology*, *105*(1), 3–41.

Sillitoe, & Mortensen. (2010). Longevity of porphyry copper formation at quellaveco, peru. *Economic Geology*, *105*(6), 1157–1162.

Sillitoe, R. H., & Perelló, J. (2005). *Andean copper province: Tectonomagmatic settings, deposit types, metallogeny, exploration, and discovery.* Society of Economic Geologist.

Smith, D. J., Naden, J., Jenkin, G. R., & Keith, M. (2017). Hydrothermal alteration and fluid ph in alkaline-hosted epithermal systems. *Ore Geology Reviews*, *89*, 772–779.

Spear, F. S., & Spear, F. S. (1993). *Metamorphic phase equilibria and pressure-temperature-time paths* (Vol. 1). Mineralogical Society of America Washington, DC.

Taillefer, A., Soliva, R., Guillou-Frottier, L., Le Goff, E., Martin, G., & Seranne, M. (2017). Fault-related controls on upward hydrothermal flow: an integrated geological study of the têt fault system, eastern pyrénées (france). *Geofluids*, *2017*.

Tosdal, R. M., & Richards, J. P. (2001). *Magmatic and structural controls on the development of porphyry cu +/- mo +/- au deposits.*

Tunick, M. H. (2010). Activation energy measurements in rheological analysis of cheese. *International Dairy Journal*, *20*(10), 680 - 685. Retrieved from http://www.sciencedirect

.com/science/article/pii/S0958694610000919 doi: https://doi.org/10.1016/j.idairyj.2010.03.010

Vicari, A., Alexis, H., Negro, C. D., Coltelli, M., Marsella, M., & Proietti, C. (2007). Modeling of the 2001 lava flow at etna volcano by a cellular automata approach. *Environmental Modelling & Software*, *22*(10), 1465 - 1471. Retrieved from http://www.sciencedirect.com/science/article/pii/S1364815206002817 (Modelling, computer-assisted simulations, and mapping of dangerous phenomena for hazard assessment) doi: https://doi.org/10.1016/j.envsoft.2006.10.005

Von Neumann, J., Burks, A. W., et al. (1966). Theory of self-reproducing automata. *IEEE Transactions on Neural Networks*, *5*(1), 3–14.

Walker, G. P. L. (1963). The breiddalur central volcano, eastern iceland. *Quarterly Journal of the Geological Society*, *119*(1-4), 29–63.

Winsberg, E. (2019). Computer simulations in science. In E. N. Zalta (Ed.), *The stanford encyclopedia of philosophy* (Spring 2019 ed.). Metaphysics Research Lab, Stanford University. https://plato.stanford.edu/archives/spr2019/entries/simulations-science/.

Wolfram, S. (1983). Statistical mechanics of cellular automata. *Reviews of modern physics*, *55*(3), 601.